EBioMedicine 72 (2021) 103625

Contents lists available at ScienceDirect

EBioMedicine

journal homepage: www.elsevier.com/locate/ebiom

Overcoming enzalutamide resistance in metastatic prostate cancer by targeting sphingosine kinase

Hui-Ming Lin[a,b], Blossom Mak[a,c,d], Nicole Yeung[a], Kevin Huynh[e], Thomas G. Meikle[e], Natalie A. Mellett[e], Edmond M. Kwan[f,g], Heidi Fettke[h,i], Ben Tran[h,i], Ian D. Davis[j,k], Kate L. Mahon[a,b,c,d,l], Alison Zhang[c], Martin R. Stockler[c,d,l,m], Karen Briscoe[n], Gavin Marx[o], Megan Crumbaker[a,b,p], Phillip D. Stricker[a,b], Pan Du[q], Jianjun Yu[q], Shidong Jia[q], Tahlia Scheinberg[a,c,d], Michael Fitzpatrick[r], Paul Bonnitcha[d,r], David R. Sullivan[l,r], Anthony M. Joshua[a,b,p], Arun A. Azad[h,i], Lisa M. Butler[s,t], Peter J. Meikle[e], Lisa G. Horvath[a,b,c,d,l,*]

[a] Garvan Institute of Medical Research, Darlinghurst, Sydney, New South Wales, Australia
[b] St Vincent's Clinical School, UNSW Sydney, Darlinghurst, New South Wales, Australia
[c] Chris O' Brien Lifehouse, Camperdown, New South Wales, Australia
[d] University of Sydney, Camperdown, New South Wales, Australia
[e] Baker Heart and Diabetes Institute, Melbourne, Victoria, Australia
[f] Department of Medical Oncology, Monash Health, Clayton, Victoria, Australia
[g] Department of Medicine, School of Clinical Sciences, Monash University, Clayton, Victoria, Australia
[h] Department of Medical Oncology, Peter MacCallum Cancer Centre, Melbourne, Victoria, Australia
[i] Sir Peter MacCallum Department of Oncology, University of Melbourne, Parkville, Victoria, Australia
[j] Cancer Services, Eastern Health, Box Hill, Victoria, Australia
[k] Eastern Health Clinical School, Monash University, Box Hill, Victoria, Australia
[l] Royal Prince Alfred Hospital, Camperdown, New South Wales, Australia
[m] Concord Repatriation General Hospital, Concord, New South Wales, Australia
[n] Mid North Coast Cancer Institute, Coffs Harbour, New South Wales, Australia
[o] Sydney Adventist Hospital, Wahroonga, New South Wales, Australia
[p] The Kinghorn Cancer Centre, St Vincent's Hospital, Darlinghurst, New South Wales, Australia
[q] Predicine, Inc., Hayward, CA, USA
[r] NSW Health Pathology, Camperdown, New South Wales, Australia
[s] Adelaide Medical School and Freemason's Centre for Male Health and Wellbeing, University of Adelaide, Adelaide, South Australia, Australia
[t] South Australian Health and Medical Research Institute, Adelaide, South Australia, Australia

ARTICLE INFO

Article History:
Received 5 September 2021
Revised 28 September 2021
Accepted 30 September 2021
Available online xxx

Keywords:
Metastatic prostate cancer
Sphingosine kinase
Enzalutamide
Ceramide

ABSTRACT

Background: Intrinsic resistance to androgen receptor signalling inhibitors (ARSI) occurs in 20–30% of men with metastatic castration-resistant prostate cancer (mCRPC). Ceramide metabolism may have a role in ARSI resistance. Our study's aim is to investigate the association of the ceramide-sphingosine-1-phosphate (ceramide-S1P) signalling axis with ARSI resistance in mCRPC.

Methods: Lipidomic analysis (~700 lipids) was performed on plasma collected from 132 men with mCRPC, before commencing enzalutamide or abiraterone. AR gene aberrations in 77 of these men were identified by deep sequencing of circulating tumour DNA. Associations between circulating lipids, radiological progression-free survival (rPFS) and overall survival (OS) were examined by Cox regression. Inhibition of ceramide-S1P signalling with sphingosine kinase (SPHK) inhibitors (PF-543 and ABC294640) on enzalutamide efficacy was investigated with *in vitro* assays, and transcriptomic and lipidomic analyses of prostate cancer (PC) cell lines (LNCaP, C42B, 22Rv1).

Findings: Men with elevated circulating ceramide levels had shorter rPFS (HR=2·3, 95% CI=1·5–3·6, $p = 0·0004$) and shorter OS (HR=2·3, 95% CI=1·4–36, $p = 0·0005$). The combined presence of an AR aberration with elevated ceramide levels conferred a worse prognosis than the presence of only one or none of these characteristics (median rPFS time = 3·9 vs 8·3 vs 17·7 months; median OS time = 8·9 vs 19·8 vs 34·4 months). SPHK inhibitors enhanced enzalutamide efficacy in PC cell lines. Transcriptomic and lipidomic analyses

* Corresponding author at: Chris O' Brien Lifehouse, 119-143 Missenden Rd, Camperdown, New South Wales 2050, Australia.
E-mail address: lisa.horvath@lh.org.au (L.G. Horvath).

https://doi.org/10.1016/j.ebiom.2021.103625

indicated that enzalutamide combined with SPHK inhibition enhanced PC cell death by SREBP-induced lipotoxicity.

Interpretation: Ceramide-S1P signalling promotes ARSI resistance, which can be reversed with SPHK inhibitors.

Research in context

Evidence before this study

Epidemiological and molecular studies indicate that dysregulated lipid metabolism is associated with prostate cancer pathogenesis and poorer clinical outcomes. Our previous studies show that elevated levels of ceramide, a type of sphingolipid, is associated with poorer clinical outcomes in prostate cancer, but this has not been examined in men with metastatic castration-resistant prostate cancer (mCRPC) receiving the novel androgen receptor signalling inhibitors (ARSI) abiraterone and enzalutamide. Other studies have demonstrated that inhibition of ceramide metabolism into pro-metastatic sphingosine-1-phosphate (S1P) has anti-cancer effects, and this has only been investigated as single agents in prostate cancer cell lines as shown by PubMed search terms for "sphingosine kinase" or "ceramide" with "anti-androgen" or "androgen signalling". The search terms of "sphingosine kinase" and enzalutamide" or "abiraterone" did not reveal any results, confirming that the combination of sphingosine kinase with enzalutamide has not been studied or reported.

Added value of this study

Our findings show that the association of elevated circulating ceramides with poorer clinical outcomes in prostate cancer also applies to men receiving ARSI for treatment of mCRPC. Additionally, we showed that the combined effect of androgen receptor gene aberrations with elevated circulating ceramides or genetic aberrations of sphingolipid metabolism was associated with poorer ARSI response in men with mCRPC. Finally, our *in vitro* work showed that combination treatment inhibiting ceramide metabolism (SPHK inhibitor) and ARSI signalling (enzalutamide) improves the efficacy of ARSI therapy, and provided a plausible mechanism of action.

Implications of all the available evidence

The findings of our study indicate that perturbations in ceramide metabolism contribute to ARSI resistance. Therefore, addition of therapy targeting the ceramide-S1P signalling axis to the standard of care ARSI therapy in mCRPC may improve clinical outcomes and should be investigated in prospective clinical trials. Patients suitable for such therapy may be identified by their plasma lipid profile.

1. Introduction

Prostate cancer (PC) is the second most common cancer and the fifth leading cause of cancer death in men worldwide [1]. In the last decade, substantial progress has been made in the treatment of metastatic castration-resistant prostate cancer (mCRPC) with the emergence of novel androgen receptor signalling inhibitor (ARSI) therapy such as enzalutamide (ENZ) and abiraterone [2–5]. However, resistance to ARSI is a major clinical challenge, with intrinsic resistance affecting 20–30% of patients, and acquired resistance being the ultimate outcome for all patients on ARSI therapy [6]. Mechanistically, ARSI resistance has been linked to androgen receptor (AR) gene aberrations such as copy number gain and mutations [7], which can be detected in circulating cell-free DNA (cfDNA) [8]. Conversely, ARSI usage can lead to the emergence of AR-negative disease, such as neuroendocrine prostate cancer which lacks targeted treatment and is invariably fatal [9]. Identifying novel therapies to overcome ARSI resistance is therefore critical to improve patient outcomes.

A novel approach to understanding ARSI resistance is to consider the role of sphingolipids, which are a class of lipids characterised by a sphingosine backbone, and regulate various biological processes including cell growth and inflammation [10–12]. Epidemiological evidence indicate that statin therapy is associated with improved overall survival (OS) in PC [13,14], which was also demonstrated for its concomitant use with abiraterone [15,16] and androgen deprivation therapy [17]. However, blood cholesterol levels were not associated with PC death [18] or risk of recurrence after radical prostatectomy [19,20], indicating that the beneficial effects of statin in PC is not necessarily related to its cholesterol-lowering mechanism. A possible alternate mechanism is the ability of statin to lower the circulating levels of ceramides, a type of sphingolipid [21–23].

Our previous lipidomic studies had shown that elevated circulating levels of ceramides were associated with earlier androgen deprivation therapy (ADT) failure in metastatic hormone-sensitive PC, shorter progression-free survival (PFS) after docetaxel in mCRPC, and shorter OS in mCRPC [24,25]. Ceramide can be metabolised into sphingosine-1-phosphate (S1P), which can promote cancer growth, metastasis and drug resistance by activating specific G-protein-coupled receptors to regulate cell proliferation, survival and the immune response [10–12]. Ceramide and S1P may also be involved in steroid synthesis and function through the regulation of steroidogenic gene transcription [26], by acting as ligands of nuclear receptors or as intracellular secondary messengers [27–29]. The liver is the main source of circulating ceramides [30], but cancer cells also express enzymes involved in *de novo* ceramide synthesis and the metabolism of ceramides into S1P, as well as S1P receptors [10]. Thus, we hypothesise that the ceramide-S1P signalling axis may be promoting poor prognosis disease in PC and may be contributing to ARSI resistance.

Metabolism of ceramides into S1P requires the conversion of ceramide into sphingosine, which is phosphorylated by sphingosine kinase (SPHK) into S1P (Fig. 1a). The ceramide-S1P signalling axis can be therapeutically targeted by chemical inhibition of SPHK to prevent the production of S1P [31]. SPHK exists as two isoforms – SPHK1 (cytoplasmic) and SPHK2 (nuclear) [32]. Various cancer tissues including PC have higher expression of SPHK1 compared to normal [33,34], where high SPHK1 expression was associated with shorter survival (no data for PC)(34). Inhibition of either SPHK1 or SPHK2 in various cancers including PC resulted in anti-tumour effects *in vitro* and *in vivo* [10,35,36]. SPHK1 inhibition also enhanced docetaxel sensitivity in PC cell lines [37]. Androgen deprivation of PC cells increased SPHK1 expression and activity, which may contribute to androgen-independent survival [38]. However, the role of SPHK as a potential target to overcome ARSI therapy resistance has not been studied.

Our study aimed to investigate the relationship between the ceramide-S1P signalling axis and ARSI resistance in mCRPC, by (Aim 1) profiling circulating lipids and *AR* aberrations in mCRPC patients

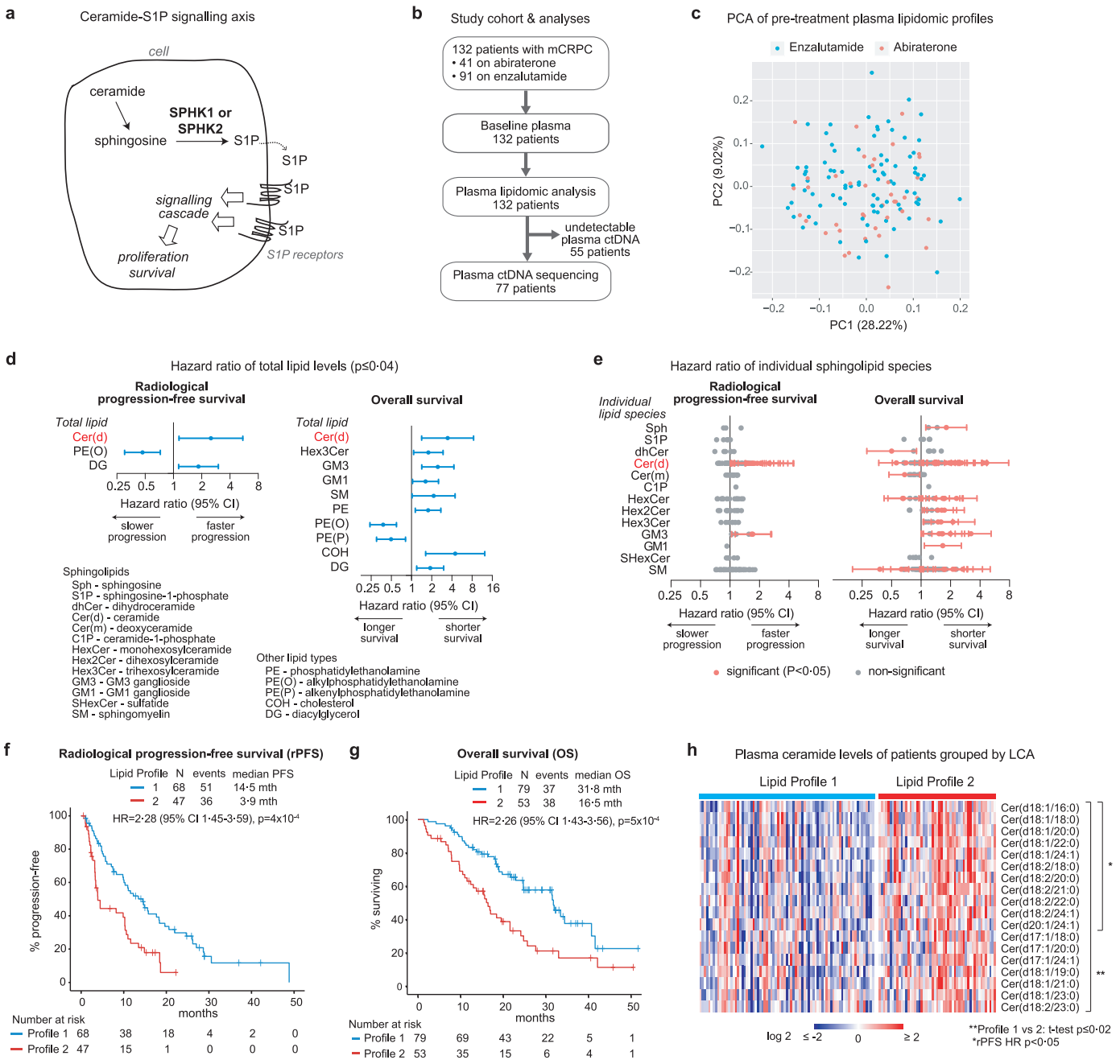

Fig. 1. Elevated pre-treatment levels of circulating ceramides are associated with ARSI resistance in mCRPC: (a) ceramide-S1P signalling axis – ceramide is metabolised into sphingosine-1-phosphate (S1P) which binds to specific receptors to activate signalling cascades that promote cell proliferation and survival; (b) outline of analyses on mCRPC study cohort; (c) scoreplot of principal components analysis (PCA) of pre-treatment plasma lipidomic profiles (each datapoint represents a plasma sample); (d) hazard ratio of total lipid levels significantly associated with rPFS or OS; (e) hazard ratio of individual levels of sphingolipid species in relation to rPFS or OS (each datapoint represents a lipid species, confidence intervals only displayed for significant lipids); (f, g) Kaplan-Meier curves of rPFS and OS of men with Lipid Profile 1 versus 2; (h) heatmap of baseline plasma levels of significant ceramide species in patients grouped by lipid profiles identified from latent class analysis (LCA).

receiving ARSI, and (Aim 2) investigating the effect of SPHK inhibitors on ENZ resistance in cell line models. We hypothesise that elevated levels of circulating ceramides and somatic aberrations in sphingolipid metabolism genes are associated with poorer response to ARSI therapy, and may be targeted by novel therapeutic combinations.

2. Methods

2.1. Patients and plasma samples

Patients with mCRPC were recruited from medical oncology clinics in academic teaching hospitals in Australia for an open-label non-interventional study investigating circulating biomarkers for any line of mCRPC treatment. The hospitals were Chris O'Brien Lifehouse, Concord Repatriation General Hospital, St Vincent's Hospital Sydney, Mid North Coast Cancer Institute, Sydney Adventist hospital, Epworth HealthCare, Monash Health, and Eastern Health. Sample size calculations estimated a minimum of 94 patients is required, as our previous study of a discovery mCRPC cohort showed that 42% have a poor prognostic lipidomic profile [24] (Type 1 error rate = 5%, deviation from true proportion = 5%); in addition, a minimum of 73 patients is required to achieve a 25% prevalence of ARSI resistance. 132 patients commencing treatment with enzalutamide or abiraterone between June 2016 to February 2020 were recruited. Patients were seen by

their clinician every two months for response assessment. Radiological progression was defined as by the Prostate Cancer Clinical Trials Working Group 2 [39].

Plasma samples were collected from these 132 patients prior to commencing treatment, according to a standardised blood collection protocol – blood was collected in EDTA-containing tubes and centrifuged at 1600 × g within 1 h of collection to separate the plasma, which was then transferred to fresh tubes and centrifuged again at 5000 × g for 10 min. Aliquots of the plasma after the second spin were stored at -70 °C until required.

2.2. Ethics

All participants provided written informed consent. The study was approved for Monash Health and Eastern Health by the Monash Health Institutional Review Board (Reference number: 15571X), and approved for the other sites by Royal Prince Alfred Hospital human research ethics committee (Reference numbers: X19-0320 & 2019/ETH12152).

2.3. Plasma lipidomic analysis

Lipidomic profiling of plasma samples was performed by liquid chromatography-mass spectrometry (LC-MS) as previously described [40]. The data was normalised using the Probabilistic Quotient Normalisation method as previously described [25], with final lipid levels transformed to logarithm-2 of pmol/ml for statistical analysis. Targeted analysis of selected lipids in the same plasma aliquots using alternative independent methods (immunoassay and targeted LC-MS) confirmed the validity of the lipidomic measurements (Supplementary Information S1.7).

2.4. Next-generation sequencing of cfDNA

Extraction of plasma cfDNA, next-generation sequencing and bioinformatics analysis was performed as previously described [41]. To summarise, extracted cfDNA underwent library preparation, panel-based hybridisation (Predicine, Inc.) and enrichment, followed by paired-end sequencing on the Illumina HiSeq Xten. Point mutations, small insertions/deletions (≤10 bp) and copy number alterations were identified using Predicine's proprietary GeneRADAR technology and DeepSea machine learning bioinformatics algorithm.

2.5. Drugs and cell lines

PF-543 (PF5), ABC294640 (ABC) and enzalutamide (ENZ) were purchased from Selleck Chemicals. All three drugs were prepared as 20 mM stocks in dimethyl sulfoxide (DMSO) and stored in aliquots at -20 °C. The drugs were diluted accordingly in culture media for *in vitro* assays, with the matching percentage of DMSO as the vehicle control treatment. PC cell lines LNCaP (RRID: CVCL_1379), C42B (RRID: CVCL_4784) and 22Rv1 (RRID: CVCL_1045) were acquired from the American Type Culture Collection (Manassas, VA, USA). The cells were cultured in RPMI 1640 containing 10% fetal bovine serum, and used in experiments between 2 and 10 passages after thawing from cryostorage. The cells were routinely tested for mycoplasma contamination (last test: 4 November 2019). The identity of cell lines were verified by analysis of microsatellite profiles (Garvan Molecular Genetics, Darlinghurst, NSW). Unless stated otherwise, cells were cultured in 6 well plates for assays with 2 ml of culture media per well, and treated with drug(s) the next day by replacing 1 ml of of the media with fresh media containing the drug(s).

2.6. Cell viability assay

Cells were seeded in 96 well plates at the following densities in 80 μl media per well: C42B – 1200 cells/well, LNCaP – 4500 cells/-well, 22Rv1 – 4500 cells/well. The next day, 40 μl of fresh media containing ENZ, PF5, ABC, or DMSO (vehicle control) were added to each well of the cultures (final volume per well = 160 μl). After 96 h, cell viability was assessed with Alamar Blue (Invitrogen) by fluorescence measurement according to manufacturer's instructions.

2.7. Colony forming assay

Cells were seeded in 6 well plates at the following densities in 2 ml media per well: C42B and 22Rv1– 500 cells/well, LNCaP – 2000 cells/well. The next day, ENZ, PF5, ABC or DMSO (vehicle control) were added to the cultures. After 1 week from seeding, culture media was refreshed without drugs. After 2 weeks from seeding, cells were fixed with 16% trichloroacetic acid for 30 min. After fixation, cells were stained with Quick Dip II (Fronine) for 30 min, and rinsed with water until the rinse was clear of excess stain. Images of the wells were taken and colonies were counted using ImageJ (National Institutes of Health, U.S.A).

2.8. Flow cytometry of apoptosis and cell cycle

Cells were seeded in 6 well plates at the following densities in 2 ml media per well: C42B – $2{\cdot}2 \times 10^5$ cells/well, LNCaP – 5×10^5 cells/well, 22Rv1 – $3{\cdot}8 \times 10^5$ cells/well. The next day, the media from each well was replaced with fresh media containing drug(s) or DMSO vehicle control. After 48 h of treatment, cells were collected for apoptosis or cell cycle analysis. Floating cells in the conditioned media were collected by centrifugation whereas adherent cells were detached with trypsin. Cells were labelling for apoptosis analysis using the AnnexinV-FITC Apoptosis Detection kit (BioVision Research Products, USA) according to manufacturer's instructions. Cells were labelled for cell cycle analysis by fixing in 70% ethanol at -20 °C for at least 24 h, followed by washing with phosphate-buffered saline (PBS), then incubation with 0.1% propidium iodide and 830 μg/ml RNase A (Sigma) for at least 4 h. Flow cytometry analyses were performed on the BD FACS Canto II system (BD Biosciences) using the FACSDiva software version 8. Data was analysed with FlowJo version 7.6.5.

2.9. Western blot

Whole cell lysates for Western Blot were prepared by scraping cells off the culture wells in RIPA lysis buffer containing protease cocktail inhibitor (Sigma Cat# P8340), cOmplete™ Mini EDTA-free protease inhibitor cocktail (Roche) and PhosStop (Roche). The cell suspension was left on ice for 15 min and then centrifuged at 17,000 ×g for 10 min at 4 °C. The supernatant (whole cell lysate) was transferred to a fresh microtube and stored at -80 °C. The protein concentration of the lysates was determined with the Bradford assay (Biorad).

Nuclear fractions were prepared by gently scraping cells off culture wells in PBS, and collecting the cells by spinning with a microcentrifuge for 10 s. The supernatant was discarded and the cell pellet was resuspended, by pipetting with a cut pipette tip, in a lysis buffer of 0.1% NP40 substitute (Sigma Cat#74385) in PBS with protease/phosphatase inhibitors as for whole cell lysates (~40 μl lysis buffer per well of a 6 well plate). The suspension was spun on the microcentrifuge for 2 min, and the pellet (nuclear fraction) resuspended in wash buffer (0.1% NP40 in PBS). The mixture was spun again for 2 min to retrieve the nuclear pellet, which was then resuspended in loading buffer (1×x mixture of 10× reducing agent, 4× sample buffer, NuPage, Invitrogen) and sonicated with a probe sonicator at

40 amplitude in 3 × 5 sec intervals. Sonicated samples were heated at 70 °C for 10 min before loading onto gels for Western Blot (5 μl sample per well).

Precision Plus Protein Dual Color Standards (BioRad) was used as the molecular weight marker. Protein gel electrophoresis of cell lysates were performed with NuPAGE 4–12% Bis-Tris Protein Gels and MOPS buffer according to manufacturer's instructions (Invitrogen), followed by transfer to PVDF membranes. After transfer, the membranes were blocked with 5% milk in Tris-buffered saline with Tween 20 (TBST) for 1 h, washed with TBST multiple times (=3 rinses repeated 4 times, 10 min soak with continuous shaking in between) and incubated in primary antibody overnight at 4 °C with continuous shaking. The next day, membranes were washed with TBST multiple times, and incubated in secondary antibodies conjugated with horse radish peroxidase (1:2000) in 5% milk for 1 h at room temperature with continuous shaking. After secondary antibody incubation, the membranes were washed with TBST multiple times, with the last wash in TBS without tween.

All primary antibodies were purchased from Cell Signaling Technology and used with the stated dilution (AR, Cat#5153, clone D6F11, rabbit, 1:1000 dilution; SPHK1, Cat#12071, RRID:AB_2797815, rabbit, 1:1000 dilution; SPHK2, Cat#32346, RRID:AB_2799021, rabbit, 1:1000 dilution; LC3B Cat#2775, RRID:AB_915950, rabbit, 1:1000 dilution; Lamin A/C, Cat#4777, RRID:AB_10545756, mouse, 1:2000 dilution) except for beta-actin (Sigma-Aldrich Cat#A5441, clone AC-15, mouse, 1:60000 dilution) and SREBP1 (Abcam Cat#ab3259, RRID: AB_303650, mouse, 1:200 dilution). Secondary antibodies were Amersham ECL Mouse or Rabbit IgG, HRP-linked whole antibody (from sheep) (Cat#NA931 & Cat#NA934, GE Healthcare Life Sciences). Antibody binding was visualised by treating the membranes with Western Lightning Plus-ECL enhanced chemiluminescence substrate (PerkinElmer) and imaging with the digital imager Fusion Fx7 (Vilber Lourmat, Germany). The primary antibody for AR has been validated by the commercial supplier, whereas those for SPHK1, SPHK2 and SREBP1 were validated by knockdown with synthetic small interfering RNA (siRNA) described below. Secondary antibodies are Amersham ECL Mouse or Rabbit IgG, HRP-linked whole antibody (from sheep) from GE Healthcare Life Sciences (Cat#NA931 & NA934).

2.10. siRNA knockdown

ON-TARGETplus SMARTpool human siRNA for *SPHK1*, *SPHK2*, *AR* and *SREBP1* (*SREBF1*) was purchased from Dharmacon. Reverse transfection was performed with the transfection reagent DharmaFECT-1 (Dharmacon) and siRNA in either 96 well plates for cell viability assays, or 6 well plates for preparation of cell lysates for Western Blotting. The transfection reagents (siRNA, DharmaFECT-1, Optimem) were mixed together, left for 20 min, and then dispensed into the wells, prior to addition of cells (reverse transfection method). After 24 h, the culture media was replaced with fresh culture media (exception: 48 h for *SPHK1* & *SPHK2*). Drug treatment or preparation of lysates for immunoblotting was performed after 48 h from the start of transfection (Day 1 = transfection, Day 3 = drug treatment or harvest). The volumes of siRNA/DharmaFECT-1/Optimem/cells per well = 10/0·07/9·93/80 μl for 96 well plate; 200/1·5/198·5/1600 μl for 6 well plate. The number of cells per well, LNCaP/C42B/22Rv1 = 9500/3000/6000 for 96 well plate; $2{\cdot}8 \times 10^5$/9×10^4/$1{\cdot}8 \times 10^5$ for 6 well plate.

2.11. Ex vivo *culture of patient-derived primary prostate tissue*

Fresh tissue cores (5 mm diameter) of surgically resected prostate were obtained from patients with localised prostate cancer undergoing radical prostatectomy at St Vincent's Private Hospital, Sydney (St Vincent Hospital's human research ethics approval reference number 12/231). The tissue cores were dissected into pieces of ~1 mm^3, and cultured on gelatine sponges (Spongostan Dental, Ferrosan Medical Devices, Soeborg, Denmark) immersed in 0.5 ml culture medium with drug(s) or matching 0·15% DMSO vehicle control [42]. After 48 h of culture, the explant tissues were formalin-fixed and paraffin-embedded (FFPE). FFPE sections (4 μM thickness) were co-immunostained with Ki67 rabbit antibody (1:500, clone SP6, Abcam Cat# ab16667, RRID:AB_302459) and p63 mouse antibody (1:100, Clone DAK-p63, Dako; marker of benign basal cells) using the Leica Bond Rx automated stainer with the ChromoPlex 1 Dual Detection kit (Leica Biosystems). The percentage of cells stained with Ki67 was quantitated by estimation.

2.12. Transcriptomic analysis of C42B cells

C42B cells were seeded in 6 well plates at $1{\cdot}4 \times 10^5$ cells in 2 ml media per well. After 3 days of growth (Day 4 if Day 1 is day of seeding), cells were treated with drug(s) or vehicle control, with 3 replicates per treatment for transcriptomic analysis. The final concentration of each drug: 10mM ENZ, 15 mM PF5, 15 mM ABC, 0.125% DMSO. After 6 h of treatment, cells were lysed with lysis buffer from the RNAeasy mini kit (Qiagen) (350 μl per well). The lysates were frozen at -70 °C and total RNA extraction was continued on another day according to the kit's instruction. RNA quality was assessed using the Agilent TapeStation system (Agilent). The cDNA synthesis, labelling and hybridisation to Human Clariom S arrays (formerly Affymetrix)(Applied Biosystems) was performed by the Ramaciotti Centre for Genomics (UNSW Sydney, Australia) with the GeneChip WT PLUS Reagent Kit as follows: starting RNA input of 100 ng per sample; hybridisation input of 2·3 μg; hybridisation conditions: 17 h, 45 °C, 60 rpm. The arrays were processed on the Affymetrix GeneChip Fluidics Station 45, and imaged with the Affymetrix Affymetrix GCS3000 scanner using the Affymetrix GeneChip Command Console (AGCC) Scan Control software (v4.0.0.1567).

2.13. Real-time polymerase chain reaction (RT-PCR)

RNA was extracted from cells cultured in 6 well plates, with Trizol Reagent (Invitrogen) according to manufacturer's instruction with additional clean-up by sodium acetate precipitation, and stored at -80 °C. RNA was converted into cDNA using the High Capacity Reverse Transcription kit (Applied Biosystems) according to manufacturer's instruction, with substitution of random primers with that from Invitrogen (#48190011, final concentration in reaction = 75 ng/μl). RT-PCR was performed on the cDNA with TaqMan Gene Expression Assays (Applied Biosystems) on Quant7 Studio (Applied Biosystems) according to the manufacturer's instruction. Gene expression levels were calculated relative to beta-actin (*ACTB*) using the comparative C_T method ($2^{-\Delta\Delta CT}$). The Taqman Gene Expression assays were Hs00358796_g1 for *DDIT3*, Hs00225520_m1 for *CHAC1*, Hs01005622_m1 for *FASN*, Hs00168352_m1 for *HMGCR*, Hs00957421_m1 for *STARD4*, Hs99999903_m1 for *ACTB*, and Hs01088679_g1 for *SREBF1*.

2.14. Lipidomic analysis of cells

Cells were trypsinised from 6-well plates and pelleted. Lysis buffer was prepared by adding fresh butylated hydroxytoulene (BHT) to Tris-NaCl buffer (20 mM Tris-HCl, 500 mM NaCl, pH 7) to achieve a final concentration of 100 μM BHT. Each cell pellet was resuspended in 200 μl of lysis buffer and homogenised by passing the cell suspension through a 30 gauge needle 20 times. Protein concentration was quantitated with the BCA protein assay kit (Pierce Biotechnology). Cell extracts equivalent to 50 μg of protein was subjected to lipid extraction with chloroform-methanol as described by Weir et al. [43]. The lipid extracts were analysed by LC-MS using the same methodology as for the plasma samples, except that the number of quantitated lipid species for LNCaP and 22Rv1 were less comprehensive

and focused mainly on cholesterol, triacylglycerol (TG) and monoalkyldiacylglycerol [TG(O)] species. Lipid levels (pmol/mg protein) were normalised using the Probabilistic Quotient Normalisation method as for the plasma lipidomic analysis, with final values expressed as log2 of pmol/mg protein for statistical analysis.

2.15. Statistics

Radiological progression-free survival (rPFS) and OS time were calculated using SPSS (version 25) as the time from the date of commencing treatment to the date of the event, and censored at the date of last follow-up if the event has not occurred. The association of plasma lipid levels with rPFS or OS was determined by univariable Cox regression (R package survival, v2.44-1.1). Unique plasma lipid profiles were identified by latent class analysis (LCA) of the levels of prognostic lipids categorised into quartiles (R package poLCA, v1.4.1) [13]. LCA is a non-supervised method that identifies class membership (lipid profiles) using the observed variables. The most parsimonious number of lipid profiles was determined with the minimum Bayesian Information criterion. Differences in plasma lipid levels between groups of patients were determined by *t*-test, which was performed with the R package multtest (v2.41.0). Principal components analysis (PCA) was performed using the R package ggfortify (v0.4.11) on pre-treatment plasma lipidomic profiles to determine if there were any underlying metabolic differences amongst the patients. Enrichment of lipid types was determined by one-sided Fisher's exact tests using the R package bc3net (v1.04).

The frequency of *AR* aberrations between groups of patients was compared by Fisher's exact test using Prism 9 (GraphPad Software). The association of *AR* aberrations, lipid profiles, or sphingolipid gene aberrations with rPFS, OS, or treatment duration was determined by univariable Cox regression as above. Median survival time was also calculated with the R package survival. Kaplan-Meier curves were drawn with the R package survminer (v0.4.6).

To identify sphingolipid genes that are associated with ARSI resistance, a list of genes associated with sphingolipid metabolism was compiled from the KEGG pathway database, NCBI Gene or literature (Supplementary S3.1). Data on copy number alterations and mRNA expression of these sphingolipid genes in mCRPC tumours from taxane-naïve patients receiving ARSI therapy and treatment duration were obtained from the genomic study by the SU2C/PCF Dream Team (Abida et al.)[44] through CbioPortal (www.cbioportal.org). Copy number alteration data with ARSI treatment duration information were available for the tumours of 108 men, of which 47 also have RNA-seq data. To overcome missing or zero values in the mRNA expression data (FPKM capture), the value of 1 was added to the mRNA expression values of all the samples, and then the dataset was transformed to log2. Cox regression and survival analyses in relation to ARSI duration were performed on men classified by copy number gain or mRNA expression (low versus high expression) of each sphingolipid gene in the presence or absence of *AR* gain, using the R package survival (v2.44-1.1).

IC50 (inhibitory concentration causing a 50% response) of ENZ dose response curves for cell lines was calculated using the log(inhibitor) vs response (three parameters) method in Prism 9. The log IC50 of two curves were compared using the Extra sum-of squares *F* test (Prism 9). *T*-tests for cell line and *ex vivo* assays were also performed with Prism 9, and are unpaired two-tail unless stated otherwise.

Microarray data was normalised with the RMA method using the Transcriptome Analysis Console (TAC) (v4.0.2, Applied Biosystems). PCA of the normalised data showed that there were 3 outliers (2 replicates of ABC & 1 replicate of ENZ, Supplementary S6.1). These outliers were excluded from the dataset and the files were re-normalised again for downstream analysis. Differentially expressed genes from the normalised data were determined using LIMMA with the TAC software. LIMMA is a moderated *t*-test for multivariable data that fits a linear model onto each variable using information from its neighbours [45]. Probes that could not be mapped to a gene were filtered from the dataset. Genes were considered to be significantly differentially expressed between compared treatments if the fold change was $\geq$1.2 fold and *p*-value $<$0.05 (unadjusted). *P*-value correction was not applied as it was too stringent and reduced the number of hits (Supplementary S6.2). Gene set enrichment analysis of differentially expressed genes was performed with the Molecular Signature Database (MSigDb) [46,47], using the "Investigate Gene Sets" module which computes the overlap between our list of differentially expressed genes and the gene sets in MsigDb. Gene symbols were used as the gene identifiers. The collection of gene sets selected were Hallmark, KEGG, and Reactome, where analyses for each collection was performed separately.

Differentially abundant lipids from lipidomic analysis of cell lines were determined using LIMMA with the R package limma (v3.41.18). Enrichment analysis of lipid types was performed with bc3net as for the plasma lipids.

Heatmaps were drawn with the R package pheatmap (v1.0.12). R version 3.6.0 was used for all analyses requiring R packages. Bar graphs were drawn with Prism 9, and represent the average $\pm$ standard error of replicates. *P*-values $<$ 0·05 were considered as statistically significant.

2.16. Role of funders

Funding sources were not involved in study design, data collection, data analysis, data interpretation or writing of the report.

3. Results

3.1. Elevated circulating ceramides are associated with ARSI resistance

To identify circulating lipids that are associated with ARSI resistance, lipidomic analysis was performed on plasma samples collected before commencement of ARSI therapy from an Australian cohort of 132 patients (Table 1, Fig. 1b). The median follow-up time of the patients was 18·5 months (1st quartile = 11·2 months, 3rd quartile = 26·5 months), with 87 radiological progression events and 75 deaths.

A total of 762 lipid species comprising 48 different lipid types were detected in the plasma samples. Principal components analysis of the pre-treatment plasma lipidomic profiles did not show any distinct groupings of the samples, indicating that there were no major variation or underlying metabolic differences between the treatment groups that may confound statistical analyses (Fig. 1c). Amongst the 48 different lipid types, only the total levels of all ceramide (Cer(d)), diacylglycerol (DG) or alkylphosphatidylethanolamine (PE(O)) species were significantly associated with rPFS (Cox regression $p \leq 0{\cdot}04$, Fig. 1d). Elevated total levels of all ceramide species were associated with shorter rPFS (HR=2·51, 95% CI 1·15−5·49, $p = 0{\cdot}02$, Fig. 1d). Elevated total levels of ceramide species or that of four other types of sphingolipids (glycosphingolipids [Hex3Cer, GM3, GM1], sphingomyelin [SM]) were associated with shorter OS (Cox regression $p \leq 0{\cdot}03$, Fig. 1d).

Assessment of the levels of individual lipid species revealed that 99 lipid species were significantly associated with rPFS (Cox regression $p < 0{\cdot}05$, Supplementary S1.1 & S1.3). Lipid species with elevated levels that were associated with shorter rPFS were significantly enriched for ceramide and diacylglycerol (Fisher's exact test $p = 0{\cdot}04$, Supplementary S1.2). Amongst all the sphingolipids, elevated levels of ceramides and GM3 gangliosides were the only species that were associated with shorter rPFS (Cox regression $p < 0{\cdot}05$, Fig. 1e). The elevated levels of several other sphingolipids including ceramides were associated with shorter OS (Cox regression $p < 0{\cdot}05$, Fig. 1e).

Table 1
Baseline characteristics of the Australian mCRPC cohort.

	Lipidomic cohort	Circulating cell-free DNA sequenced sub-cohort
Total number of men	132	77
Treatment		
Enzalutamide	91 (69%)	52 (68%)
Abiraterone	41 (31%)	25 (32%)
Age (years), median [Q1, Q3]	74 [67, 81]	74 [67, 80]
Follow-up, months [Q1, Q3]	18 [11, 26]	18 [9,25]
Status at censoring		
Alive	57 (43%)	35 (45%)
Dead	75 (57%)	42 (55%)
Gleason grade at diagnosis		
≤6	6 (5%)	2 (3%)
7	25 (19%)	11 (14%)
8	19 (14%)	12 (16%)
≥9	58 (44%)	38 (49%)
unknown	24 (18%)	14 (18%)
Prostate-specific antigen (ng/mL), median [Q1, Q3]	28 [9, 66]	19 [6, 83]
Haemoglobin (g/L), median [Q1, Q3]	127 [118, 137]	126 [118, 138]
Alkaline phosphatase (U/L), median [Q1, Q3]	105 [76, 171] 0·8% missing data	102 [73, 176]
Albumin (g/L), median [Q1, Q3]	38 [35, 41] 0·8% missing data	38 [35, 41]
ECOG performance status		
0	40 (30%)	24 (31%)
1	82 (62%)	46 (60%)
2	10 (8%)	7 (9%)
Metastasis		
Bone	113 (86%)	64 (83%)
Visceral	12 (9%)	6 (8%)
Primary treatment		
Surgery	30 (23%)	21 (28%)
Radiation ± ADT	27 (21%)	11 (14%)
Primary ADT	7 (5%)	3 (4%)
Metastatic disease at diagnosis	65 (49%)	41 (53%)
No primary treatment	3 (2%)	1 (1%)
Prior treatment exposure		
Prior chemotherapy only	42 (32%)	31 (40%)
Prior ARSI only	5 (4%)	0 (0%)
Prior chemotherapy and ARSI	6 (5%)	4 (5%)
Line of ARSI treatment		42 (55%)
First	79 (60%)	
Second	45 (34%)	30 (39%)
Third	6 (5%)	5 (6%)
Fourth	1 (0·8%)	0 (0%)
Fifth	1 (0·8%)	0 (0%)

Definition of abbreviations: Q1, 1st quartile; Q3, 3rd quartile; ADT, androgen deprivation therapy

Latent class analysis (an unsupervised analysis) of the 102 lipid species associated with rPFS was performed to further demonstrate the prognostic role of circulating ceramide levels. The analysis classified the patients into two groups with different prognoses, referred to as Lipid Profiles 1 and 2. Patients with Lipid Profile 2 had shorter rPFS (HR=2·28, 95% CI=45−3·59, p = 0·0005) and shorter OS (HR=2·26, 95% CI=1·43−3·56, p = 0·0005) than patients with Lipid Profile 1 (Fig. 1f & g). Additionally, patients with Lipid Profile 2 had higher levels of several ceramide species (two-tail t-test $p < 0·05$, Fig. 1h, Supplementary S1.3) including Cer(d18:1/24:1), a key component of our previously identified circulating lipid signature in docetaxel-treated mCRPC [24,25].

Fifteen patients receiving ENZ and five patients receiving abiraterone also had plasma samples collected at the time of progression. These plasma samples were subjected to lipidomic analysis together with the baseline samples. Although treatment-specific effects on the lipidomic profiles cannot be conclusively determined with such a small number of patients, differences in the levels of 84 lipids were identified between both treatments (Supplementary S1.5). The levels of dehydrocholesteryl ester, alkenylphosphatidylethanolamine and dehydrodesmosteryl ester were lower in plasma from ENZ-treated patients, whereas the levels of oxidised lipids and dihydroceramide were higher. However, the total levels of ceramide were not significantly different between both treatments (ENZ/abiraterone fold difference = 1·099, t-test p = 0·44).

Overall, our lipidomic analysis showed that elevated circulating ceramides were associated with ARSI resistance in mCRPC patients.

3.2. *Elevated circulating ceramides are associated with worse prognosis in the presence of* AR *gene aberrations*

Somatic *AR* gene aberrations were determined through next-generation sequencing of cfDNA of the baseline plasma samples (Predicine, Inc. [41]). Only 77 of the 132 patients had detectable cfDNA for sequencing. This subset of patients had similar clinical characteristics to the full cohort (Table 1). Somatic *AR* gene aberrations were found in 33 of these 77 patients (43%), and consisted of gains (26 patients, 34%) and missense mutations (12 patients, 16%) (Fig. 2a, Supplementary S2.1). Consistent with previous studies [7,41], the presence of any of these *AR* aberrations was associated with shorter rPFS (HR=2·10, 95% CI 1·16−3·79, p = 0·01), shorter prostate-specific antigen-progression-free survival (HR=2·40, 95% CI=1·41−4·08, p = 0·001), decreased treatment duration (HR=2·26, 95% CI=1·35−3·80, p = 0·002) and shorter OS (HR=3·62, 95% CI=1·88−6·97, $p < 0·001$).

The circulating levels of 17 ceramide species were higher in patients with *AR* aberrations than those without, and 12 of these ceramide species were also elevated amongst patients with the poor prognostic Lipid Profile 2 (Fig. 2b, two-tail t-test $p < 0·05$, Supplementary S2.2). Furthermore, *AR* aberrations were more frequent in patients with Lipid Profile 2 compared to those with Lipid Profile 1 (58% vs 33%, Fisher's exact test p = 0·04) (Fig. 2c), indicating that *AR* aberrations are enriched in patients with Lipid Profile 2.

The clinical outcomes of having both Lipid Profile 2 and any *AR* aberration were assessed. Patients having both Lipid Profile 2 and any *AR* aberration (Group C) had significantly shorter rPFS and significantly shorter OS than those having Lipid Profile 1 without an *AR* aberration (Group A) (rPFS: median Group A vs C =17·7 vs 3·9 months, HR=2·66, p = 0·002; OS: median Group A vs C = 34·4 vs 8·9 months, HR=6·83, $p < 0·001$)(Fig. 2d, e, Supplementary S2.3). Patients having both Lipid Profile 2 and any *AR* aberration (Group C) also had shorter rPFS and significantly shorter OS than those having either Lipid Profile 2 or *AR* aberration (Group B) (rPFS: median Group C vs B = 8·3 vs 3·9 months, HR=1·47, p = 0·28; OS: median Group C vs B = 19·8 vs 8·9 months, HR=2·23, p = 0·02)(Fig. 2d, e, Supplementary S2.3).

Overall, elevated circulating ceramides and *AR* aberrations were individually associated with worse clinical outcomes with ARSI treatment, and having both of these characteristics conferred a much poorer prognosis.

3.3. *Sphingolipid gene aberrations are associated with ARSI resistance in the presence of* AR *gain*

We next investigated whether somatic aberrations in genes involved in sphingolipid metabolism were associated with ARSI resistance, by using open-access tumour genomic data of taxane-naïve mCRPC patients receiving ARSI therapy in the United States [44], available on cBioPortal. We examined copy number alterations and mRNA expression of 65 sphingolipid genes in the dataset, consisting of 108 patients with tumours profiled by whole-exome sequencing, of which 47 were also profiled by RNA-seq. The length of time that the patients received ARSI treatment was the only indicator of ARSI resistance available for this cohort. *AR* gain (high level) was

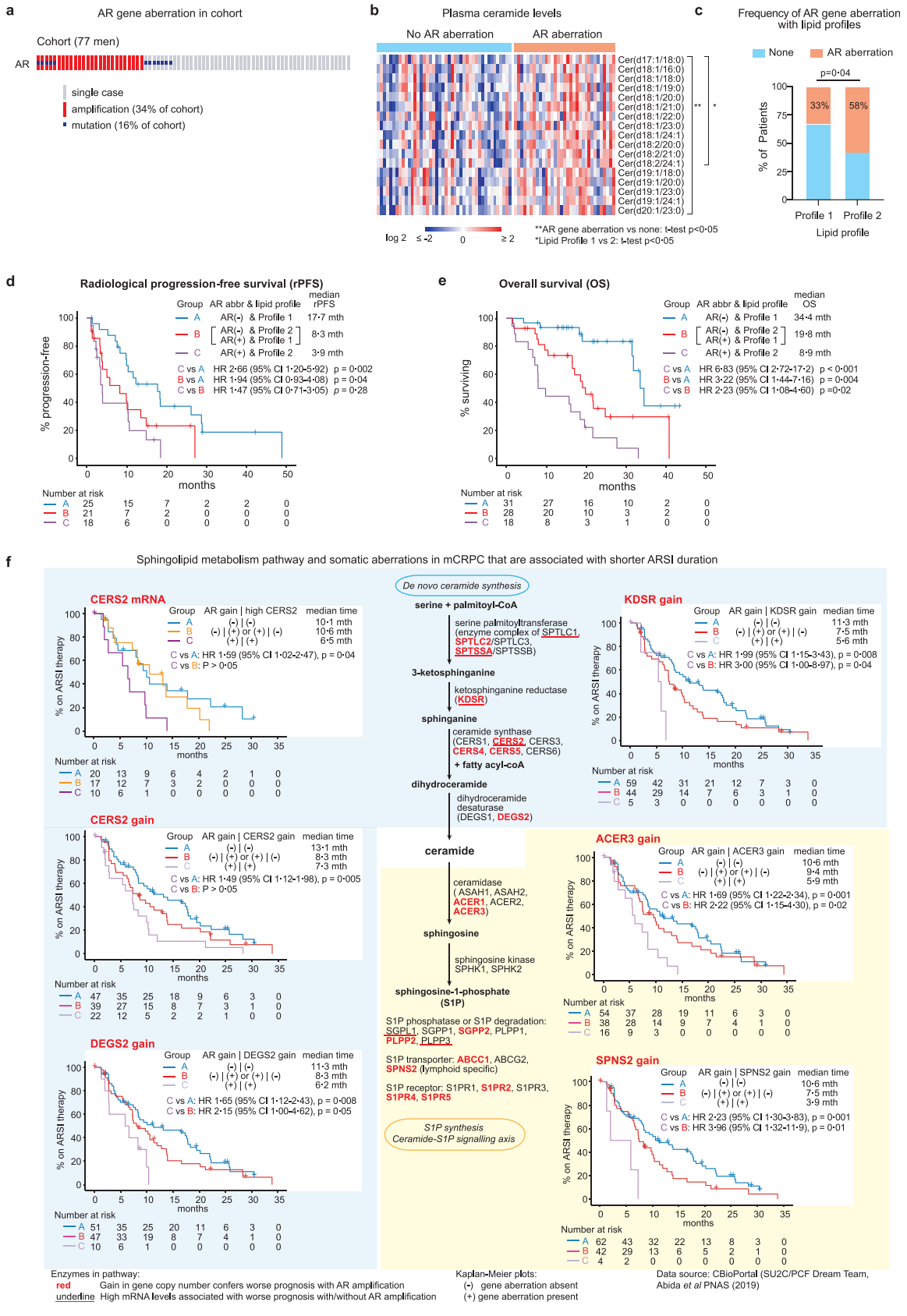

Fig. 2. Elevated circulating levels of ceramides and somatic aberrations of sphingolipid genes are associated with worse response to ARSI in the presence of AR aberrations: (a) AR aberrations in mCRPC study cohort; (b) heatmap of plasma levels of ceramide species in patients grouped by AR aberration status; (c) percentage of patients with AR aberrations according to lipid profile; (d & e) Kaplan-Meier curves of rPFS and OS of patients grouped by AR aberration status and Lipid Profile 2; (f) metabolic pathway of de novo ceramide synthesis and ceramide-S1P signalling axis with sphingolipid gene aberrations (red = copy number gain; underlined = high mRNA) that are associated with worse ARSI treatment duration in the presence of AR aberrations, and examples of their Kaplan-Meier curves.

associated with shorter duration of ARSI treatment (HR=1·28, 95% CI=1·03−1·58, $p = 0·02$).

Copy number gain (low and high level) or elevated mRNA expression of six sphingolipid-related genes were significantly associated with shorter ARSI treatment duration in men with mCRPC (Supplementary S3.2, Cox regression $p < 0·05$). However, men having both *AR* gain and copy number gain of any of 26 sphingolipid genes have shorter ARSI treatment duration compared to men with none of these genetic aberrations (Cox regression $p < 0·05$, Fig. 2f [Group C vs A], Supplementary S3.3). Sixteen of these 26 sphingolipid genes are involved in the ceramide-S1P signalling axis and *de novo* ceramide synthesis (Fig. 2f). Men who had both *AR* gain and copy number gain of any of 9 of these 26 sphingolipid genes also had significantly shorter ARSI treatment duration compared to men with only one of these genetic aberrations (Cox regression $p \leq 0·05$, Fig. 2f [Group C vs B], Supplementary S3.3). Five of these 9 sphingolipid genes are involved in the ceramide-S1P signalling axis and *de novo* ceramide synthesis – *KDSR, ACER3, SPNS2, PLPP2, S1PR4*.

Elevated mRNA expression of five sphingolipid genes also conferred shorter ARSI treatment duration if any were present with *AR* gain, compared to the absence of both genetic aberrations (Cox regression $p < 0·05$, Supplementary S3.4). Four of these genes were amongst the 26 with copy number gain that were associated with shorter ARSI duration in the presence of *AR* gain – *CERS2, SPTSSA, GLB1, GBA*.

Overall, these associations suggest that copy number gain or elevated mRNA expression of sphingolipid genes in mCRPC tumours may be mediating ARSI resistance induced by *AR* gain through enhanced ceramide-S1P signalling from increased *de novo* ceramide synthesis, conversion of ceramide into S1P and expression of S1P receptors.

3.4. *SPHK inhibition enhances ENZ efficacy* in vitro

To investigate the potential contribution of the ceramide-S1P signalling axis to ENZ resistance in tumour cells, AR-positive PC cell lines LNCaP, C42B and 22Rv1 were treated with ENZ alone or in combination with the SPHK inhibitors, PF-543 (PF5) or ABC294640 (ABC), which inhibit SPHK1 and SPHK2, respectively (Fig. 3a). All three cell lines express AR, SPHK1 and SPHK2 (Fig. 3b). However, C42B and 22Rv1 exhibit greater resistance to ENZ than LNCaP (Fig. 3c). Both SPHK inhibitors reduced PC cell viability, but their effects were greater when combined with ENZ (t-test $p < 0·0001$, Fig. 3d). Both SPHK inhibitors also significantly decreased the IC50 of ENZ in all three cell lines (F-test $p < 0·008$, Fig. 3e), except for PF5 treatment of LNCaP. The combined treatments of ENZ with either SPHK inhibitor also resulted in significantly less colony formation than individual treatments (one-tail *t*-test $p < 0·05$, Fig. 3f).

ENZ and SPHK inhibition reduced cell viability by decreasing cell proliferation and/or enhancing apoptosis or necrosis, depending on the cell line (t-test $p < 0·05$, Fig. 3g). ABC alone (SPHK2 inhibition) or in combination with ENZ caused a higher percentage of LNCaP and C42B cells to remain in the G1 phase compared to control or ENZ treatment (t-test $p \leq 0·02$). PF5 (SPHK1 inhibition) caused a higher percentage of LNCaP cells to remain in the G1 phase compared to control treatment (t-test $p = 0·009$). Either SPHK inhibitor alone or in combination with ENZ increased apoptosis/necrosis in all three cell lines, compared to ENZ or control treatment (t-test $p < 0·05$). PF5 induced autophagy in 22Rv1, which is demonstrated by the conversion of LC3B-I into LC3B-II (Fig. 3h), indicating that 22Rv1 also undergoes autophagic cell death in response to SPHK1 inhibition. AR levels were not altered by the SPHK inhibitors or ENZ treatment in any of the cell lines (Supplementary S4.4).

Transient knock-down of AR expression with synthetic small interfering RNA (siRNA) in combination with either SPHK inhibitor also resulted in decreased cell viability in all three cell lines (Supplementary S5), thus confirming that inhibition of AR signalling in combination with SPHK inhibition decreases cell viability.

3.5. *SPHK inhibition enhances ENZ efficacy* ex vivo

The efficacy of SPHK inhibition in overcoming intrinsic ENZ resistance in prostate tissues was determined by treating *ex vivo* cultures of fresh tissue biopsies of the prostate from 14 patients with localised PC undergoing radical prostatectomy. After 48 h of culture in ENZ and PF5 or ABC, the proliferation of cancer cells and adjacent benign cells were assessed by Ki67 immunostaining and compared to control (DMSO vehicle). Explants from 11 patients showed increased Ki67 expression with ENZ treatment compared to control (DMSO vehicle) (Fig. 3i). SPHK inhibitors prevented the ENZ-induced increase in Ki67 expression (paired one-tail *t*-test $p \leq 0·003$, Fig. 3i), suggesting that SPHK inhibition can overcome ENZ resistance in prostate cancer tissue.

3.6. *ENZ combined with SPHK inhibition enhances ER stress and lipogenesis gene expression*

To further investigate the mechanism of SPHK inhibition on enhancing ENZ efficacy, transcriptomic analysis with Clariom D (Affymetrix) microarrays was performed on C42B cells treated for 6 h with ENZ, SPHK inhibitors (ABC or PF5) or vehicle control (DMSO). This early timepoint was chosen to identify changes in gene expression and signaling pathways prior to apoptosis and cell death processes.

Gene set enrichment analysis was performed on differentially expressed genes to identify the relevant cellular functions and signalling pathways (Supplementary S6.3, S6.4). As expected, androgen-regulated genes were downregulated by ENZ treatment (LIMMA $p < 0·05$, Supplementary S6.3 & S6.4), indicating that AR is still responsive to ENZ despite C42B being more resistant to ENZ than the parental cell line, LNCaP. The separate contribution of ENZ and SPHK inhibition to the combination treatments was dissected by examining the overlap of differentially expressed genes from the comparisons of "ENZ versus control", "SPHK inhibition versus control" and "combination treatment versus ENZ" (Fig. 4a, Supplementary S6.3 & S6.4). The analyses indicated that upregulation of lipid metabolism and endoplasmic reticulum (ER) stress genes were, respectively, driven by SPHK1 inhibition (PF5) and ENZ in the combination treatment (Fig. 4a).

The expression of representative lipid metabolism genes (*FASN, STARD4, HMGCR)* and ER stress genes (*DDIT3, CHAC1*) was validated using Real-Time Polymerase Chain Reaction (RTPCR) in all three cell lines (Fig. 4b). PF5 alone and combined with ENZ upregulated the expression of all three lipid metabolism genes compared to ENZ alone after 6 or 24 h of treatment in all three cell lines (*t*-test $p \leq 0·04$, Fig. 4b). ENZ-ABC only increased the expression of *FASN* in C42B and *HMGCR* in 22Rv1 compared to ENZ after 24 h treatment (*t*-test $p \leq 0·04$, Fig. 4b). ENZ generally decreased the levels of *HMGCR* and *STARD4*, and opposed their upregulation by PF5 or ABC.

ENZ-PF5 enhanced the expression of both ER stress genes compared to ENZ alone in C42B and 22Rv1 (*t*-test $p \leq 0·04$), but not LNCaP after 6 or 24 h treatment (Fig. 4c). ENZ-ABC enhanced the expression of both ER stress genes compared to ENZ alone, in all three cell lines after 6 or 24 h treatment (t-test $p \leq 0·04$, Fig. 4c). PF5, ABC or ENZ alone was sufficient to upregulate the expression of the ER stress genes compared to control treatment, but their upregulation was further increased by combination treatment (t-test $p < 0·04$, Fig. 4c).

Overall, the transcriptomic data indicate upregulation of lipid synthesis pathways and ER stress by concurrent SPHK inhibition with ENZ treatment. SPHK1 inhibition (PF5) appears to have a stronger effect on upregulation of lipid synthesis pathways than SPHK2 inhibition (ABC).

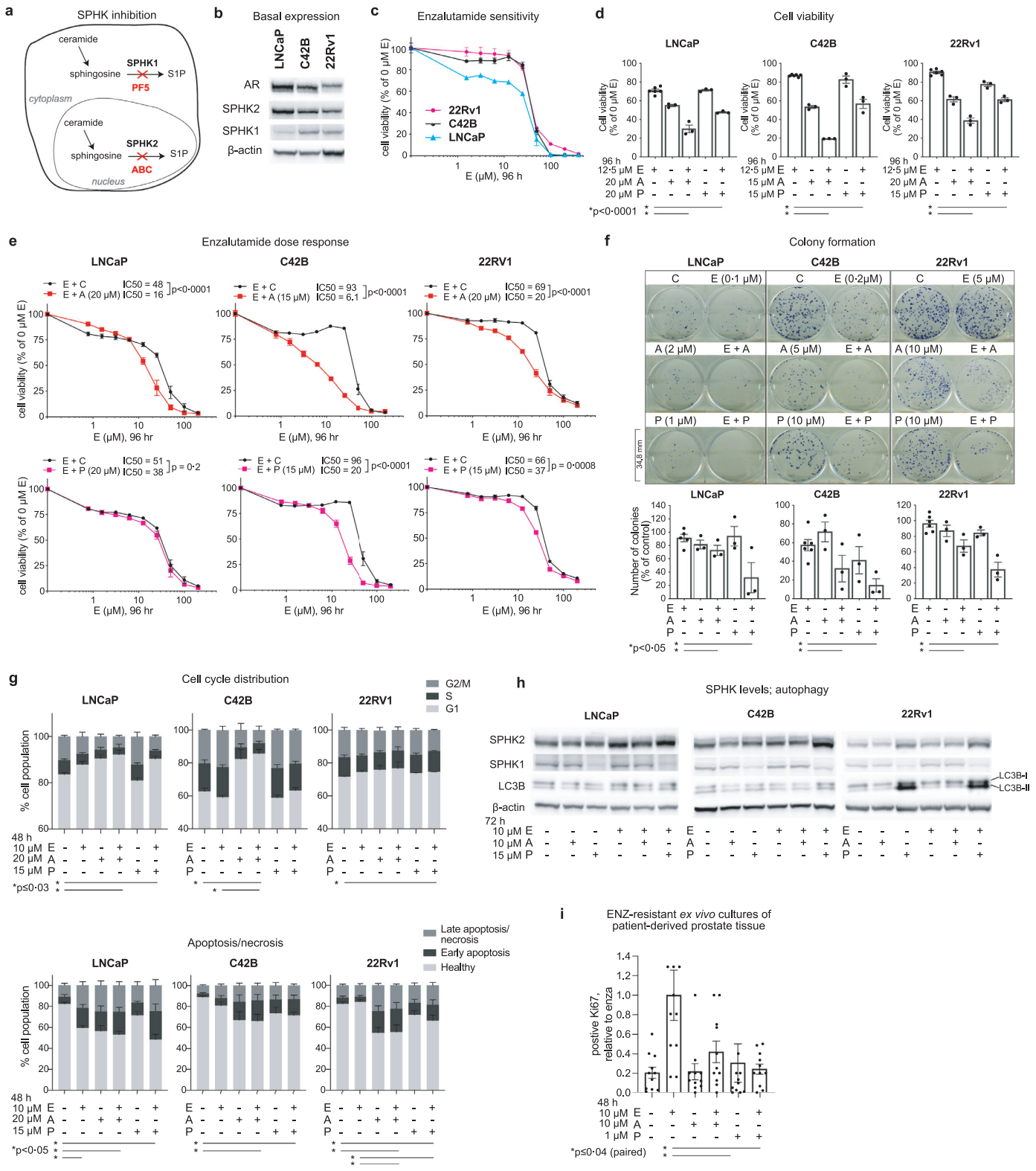

Fig. 3. ENZ-SPHK inhibition reduces viability of prostate cancer cells (figure abbreviations: C, vehicle control; E, ENZ; P, PF5; A, ABC): (a) sphingosine kinase (SPHK) inhibition – PF5 inhibits SPHK1 which is present in the cytoplasm, whereas ABC inhibits SPHK2 which is predominantly present in the nucleus, thus blocking the conversion of sphingosine into S1P; (b) representative Western blot confirming the expression of AR, SPHK1 and SPHK2 (original whole blot displayed in Supplementary S4); (c) ENZ dose-response curves demonstrating differences in sensitivity of the cell lines; (d) cell viability after 96 h treatment of SPHK inhibitors ± ENZ, *t-test $p < 0{\cdot}0001$; (e) ENZ dose-response curves of combination treatment; (f) representative photos of colony formation, and number of colonies formed after treatment with SPHK inhibitors ± ENZ, *one-tail t-test $p < 0.05$; (g) distribution of cell cycle phases and percentage of apoptotic/necrotic cells after 48 h treatment with SPHK inhibitors ± ENZ, *t-test $p \leq 0{\cdot}05$ for at least one of the subsets; (h) representative Western blots of SPHK1, SPHK2 and LC3B (original whole blots displayed in Supplementary S4); (i) percentage of Ki67 in explants cultured from fresh primary prostate tumours of 11 patients (mean ± standard error), *paired t-test $p \leq 0{\cdot}04$. Dose response curves and bar graphs are mean ± standard error of 3-4 replicates unless shown otherwise. P-values are calculated by two-tail t-test, unless stated otherwise.

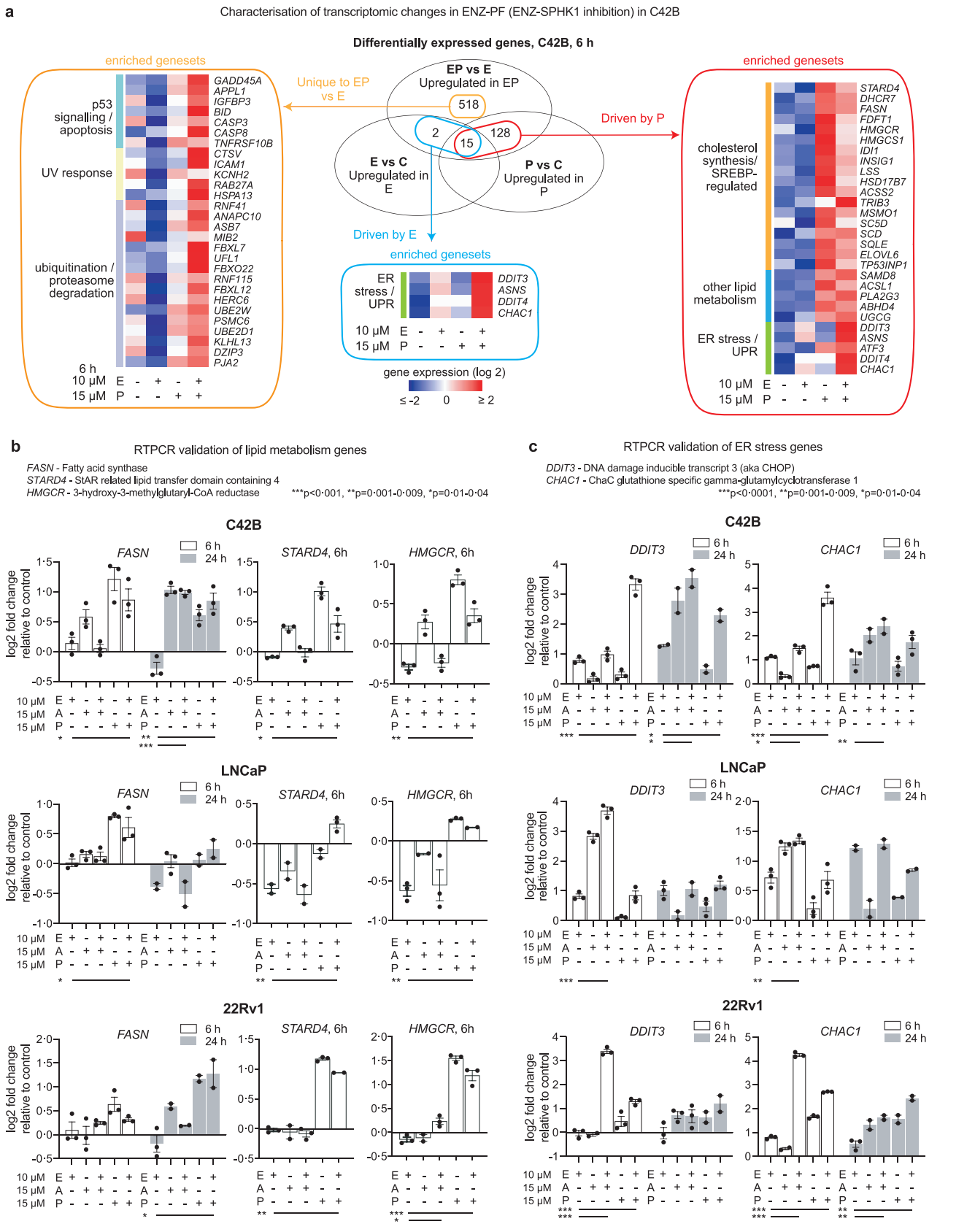

Fig. 4. Transcriptomic changes induced by ENZ-SPHK inhibition in cell lines (figure abbreviations: C, vehicle control; E, ENZ; P, PF5; A, ABC): (a) Venn diagram of upregulated genes in C42B treated with ENZ, PF5 or control for 6 h, and heatmap of the expression of enriched genes from the Venn diagram partitions; (b) & (c) RTPCR quantitation of representative genes associated with lipid metabolism and ER stress in C42B, 22Rv1 and LNCaP cells after 6 or 24 h treatment. *P*-values are from two-tail *t*-tests. Bar graphs are mean ± standard error.

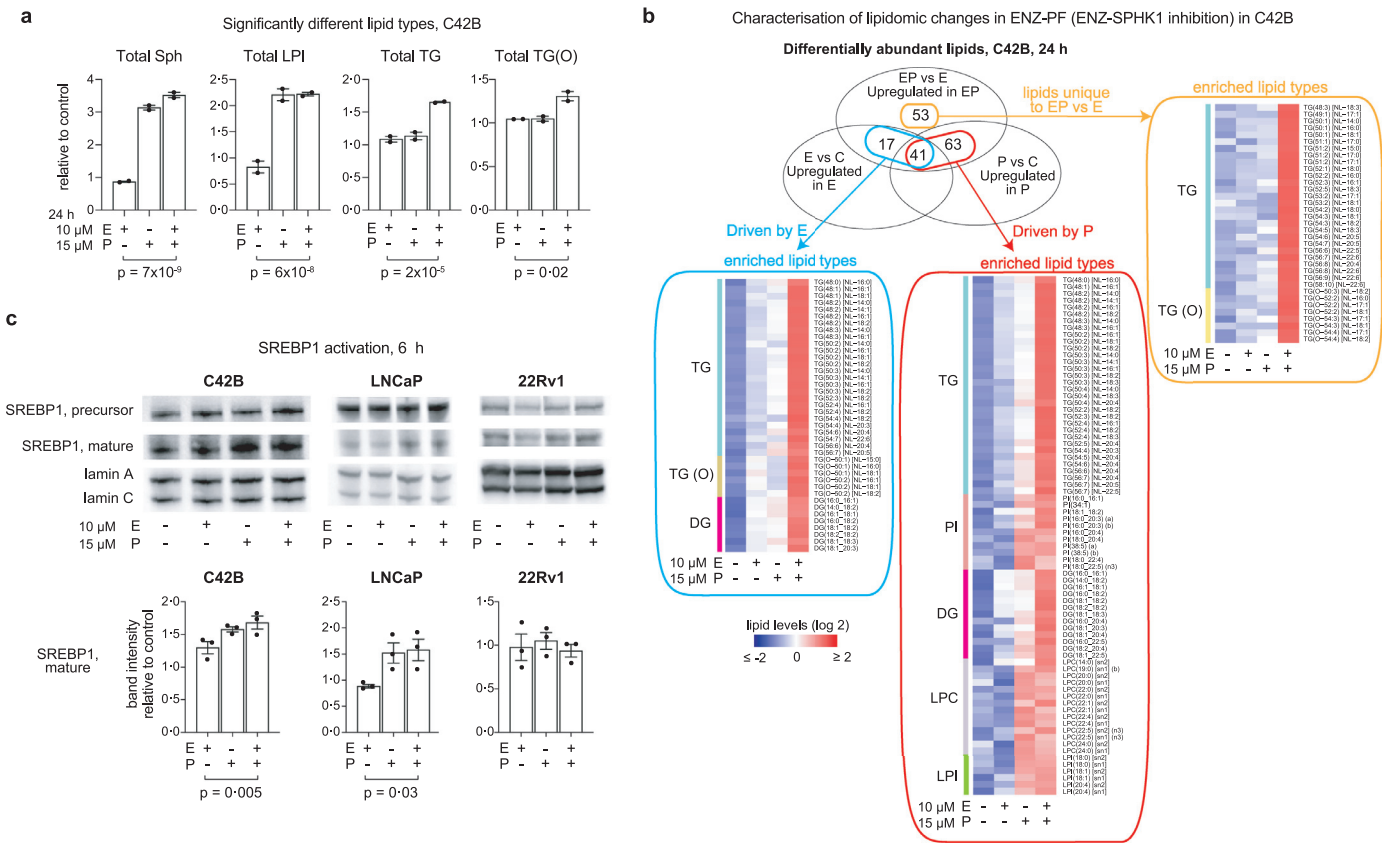

Fig. 5. Lipidomic changes induced by ENZ-SPHK1 inhibition (PF5) and the proposed mechanism of the treatments (abbreviations in figures: E, ENZ; P, PF5; Sph, sphingosine; DHT, dihydrotestosterone; AR, androgen receptor; TG, triacylglycerol): (a) lipid types with significantly increased total levels in C42B cells after 24 h treatment (LIMMA *p*-values); (b) Venn diagram of abundant lipids in C42B treated with ENZ, PF5 or control for 24 h, and heatmap of the levels of enriched lipids from the Venn diagram partitions; (c) representative Western blots of SREBP1 activation after 6 h treatment, and densitometry analyses of the bands (one-tail paired *t*-test; whole western blots with markers are diplayed in Supplementary S9. Bar graphs are mean ± standard error).

3.7. ENZ combined with SPHK inhibition increases triacylglycerol levels

Given that ENZ and SPHK inhibitors altered the expression of lipid synthesis genes, we next determined which lipids were affected by performing lipidomic analysis (764 lipid species) of C42B cells treated for 24 h with ENZ, PF5, ABC or DMSO vehicle control. As expected, SPHK1 inhibition by PF5 and ENZ-PF5 increased the total levels of sphingosine in C42B compared to control (LIMMA $p < 0{\cdot}0001$, Fig. 5a), consistent with the inhibition of sphingosine phosphorylation. However, accumulation of sphingosine was not observed for ABC or ENZ-ABC treatment (Supplementary S7.3). Although S1P was measured, changes were not detected in any of the treatments, possibly due to its extracellular release and characteristically short half-life [48].

Compared to ENZ treatment, ENZ-PF5 (SPHK1 inhibition) significantly increased the total levels of lysophosphatidylinositol (LPI), triacylglycerol (TG) and monoalkyldiacylglycerol [TG(O)], whereas ENZ-ABC (SPHK2 inhibition) only increased the total levels of TG (LIMMA $p \leq 0{\cdot}02$; Fig. 5a, Supplementary S7.2, S7.3). Enrichment analysis of individual lipid species showed that the lipids upregulated by ENZ-PF5 compared to ENZ were significantly enriched for TG, TG(O), diacylglycerol (DG), LPI and phosphatidylinositol (PI) (Fisher's exact test $p < 0{\cdot}05$, Supplementary S7.4). Upregulation of these lipid types is consistent with enhanced synthesis of TG, as DG is a precursor of TG, whereas LPI and PI share the same phosphatidic acid precursor as DG (Supplementary S7.5).

The separate contribution of ENZ and PF5 to the lipidomic changes caused by combination treatment were dissected by examining the overlap of differential lipids from the comparisons of "ENZ versus control", "PF5 versus control" and "ENZ-PF5 versus ENZ". The analysis showed that ENZ or PF5 treatments alone was sufficient to increase the levels of TG, with an even higher increase by ENZ-PF5 combination (LIMMA $p < 0{\cdot}05$, Fig. 5b). The ENZ-PF5 combination also increased the levels of additional TG species that was not enhanced by either individual treatment (LIMMA $p < 0{\cdot}05$, Fig. 5b). The number of TG species upregulated by ENZ-ABC compared to ENZ was much lower than that for ENZ-PF5 (Supplementary S7.6).

Although transcriptomic analysis and RT-PCR validation showed enhanced expression of cholesterol synthesis genes by ENZ-PF5 combination in C42B cells, the levels of free cholesterol were not altered.

A targeted lipidomic analysis was then performed on LNCaP and 22Rv1 to examine the levels of TG, TG(O) and cholesterol, after 24 h of treatment with SPHK inhibition and ENZ. In contrast to C42B, total TG levels were not altered by PF5, ABC or combination with ENZ. Instead, cholesterol levels were increased by PF5 and ENZ-PF5 compared to ENZ in both cell lines, whereas TG(O) levels were elevated by ENZ-PF5 and ENZ-ABC compared to ENZ in LNCaP (t-test $p \leq 0{\cdot}04$, Supplementary S8).

Overall, these findings indicate that combined ENZ and SPHK treatment increased lipid synthesis and accumulation which may be causing lipotoxicity-induced cell death, where the type of accumulated lipids vary according to the cell lines.

3.8. ENZ combined with SPHK1 inhibition increases SREBP activation

Transcriptomic and lipidomic analysis demonstrated that SPHK inhibitors alone and in combination with ENZ enhanced lipogenesis in the PC cell lines. Several of the lipid synthesis genes are known to

be regulated by SREBPs (sterol regulatory-element binding proteins) (Fig. 4a), which are transcription factors that stimulate lipogenesis gene expression [49]. Proteolytic cleavage of SREBP into a mature active form is required for transcription. SREBP1 stimulates both lipogenic and cholesterogenic gene expression, whereas SREBP2 regulates cholesterogenic expression.

To determine if enhanced SREBP activity contributes to ENZ-SPHK inhibition-induced lipogenesis, the expression of SREBP1 and SREBP2 in PC cells treated with ENZ, PF5, ABC or vehicle control for 6 h were analysed by Western blot. ENZ-PF5 (SPHK1 inhibition) treatment increased the levels of mature SREBP1 compared to ENZ alone in C42B (one-tail paired *t*-test $p = 0{\cdot}005$) and in LNCaP (one-tail paired *t*-test $p = 0{\cdot}03$)(Fig. 5d), but not in 22Rv1 cells (one-tailed paired *t*-test $p = 0{\cdot}41$). The levels of mature SREBP1 in PF5 or ENZ-PF5 treated C42B cells were also higher than that of control (one-tail *t*-test $p = 0{\cdot}002$ and 0·01, respectively). ENZ-ABC (SPHK2 inhibition) only increased the levels of mature SREBP1 in LNCaP compared to ENZ (one-tail paired *t*-test $p = 0{\cdot}007$, Supplementary S9.2).

Overall, these findings suggest that ENZ-PF5 (SPHK1 inhibition) induced-lipogenesis in C42B and LNCaP is mediated by increased SREBP1 activation, whereas a different mechanism of enhanced lipogenesis is operating in 22Rv1.

4. Discussion

Treatment resistance to ARSI remains a significant clinical problem for men with mCRPC. Our study has demonstrated that a circulating lipid profile consisting of elevated levels of ceramides is associated with shorter rPFS on ARSI treatment and somatic *AR* aberrations. Furthermore, having both *AR* aberrations and a lipid profile of elevated ceramides confer a much poorer prognosis with regards to both rPFS and OS. Likewise, having both *AR* gain and somatic gene aberrations in sphingolipid metabolism in mCRPC tumour tissue significantly reduces ARSI treatment duration. These associations indicate that ARSI resistance is mediated not only by genetic anomalies in *AR*, but also by perturbations in sphingolipid metabolism, and thus patients may benefit from combination therapy targeting both AR signalling and sphingolipid metabolism. Indeed, our study demonstrated that targeting the ceramide-S1P signalling axis by chemical inhibition of SPHK1 or SPHK2 can enhance the efficacy of ENZ through increased cancer cell death.

Elevation of circulating ceramides in men with poorer prognosis observed in our study could be a bystander effect of enhanced liver/tumour production; and/or could be contributing to ARSI resistance and tumour progression through their uptake by the tumour followed by conversion into pro-survival S1P. In support of the latter, we found that increased mRNA expression or copy number gain of genes related to the ceramide-S1P signalling axis in mCRPC tumours were associated with shorter ARSI treatment duration especially in the presence of *AR* gain. Regardless of the source of the circulating ceramides, their increased levels are associated with poorer prognosis especially in the presence of *AR* aberrations, suggesting that the ceramide-S1P signaling axis promotes ARSI resistance and is a potential therapeutic target in mCRPC.

Several studies have demonstrated that inhibition of S1P production by SPHK can decrease cancer growth [10,36,50,51]. Sphingosine itself is pro-apoptotic, thus its accumulation from SPHK inhibition may be triggering apoptosis [52]. However, our study showed that the enhanced cell death by the combination of ENZ with SPHK inhibition may be occurring through enhanced ER stress and lipogenesis, with the latter mediated by SREBP1 in the case of SPHK1 inhibition by PF5. The ER is the main site of lipid synthesis and protein folding. Disruption of ER homeostasis, such as accumulation of unfolded proteins and alterations in ER lipid composition, causes ER stress and activates the unfolded protein response to restore homeostasis [53]. Failure to restore ER homeostasis results in apoptosis and cell death [53]. Our study showed that SPHK inhibition or ENZ treatment alone was sufficient to upregulate the expression of ER stress genes compared to vehicle control. ER stress could be a survival mechanism of ENZ resistance as Sheng *et al* (2019) showed that AR signalling activated MYC signalling through the unfolded protein response to promote PC cell growth [54]. SPHK inhibition may be causing ER stress through the accumulation of sphingosine, as sphingosine and SPHK inhibition can disrupt endocytic membrane trafficking [55]. Increased activation of lipogenesis genes and enhanced levels of triacylglycerol or cholesterol by SPHK1 inhibition (PF5) in PC cells in our study is consistent with other reports that ER stress can induce SREBP-mediated lipotoxicity [56,57]. Therefore, the intensification of ER stress from both SPHK inhibition and ENZ may be causing the unfolded protein response to activate apoptosis instead of restoring homeostasis.

The connection between sphingolipid metabolism and triacylglycerol metabolism has been demonstrated by studies on mice with S1P-lyase (SGPL1) [58] or acid sphingomyelinase (ASM) deficiency [59]. SGPL1 degrades S1P, whereas ASM (aka SMPD1) hydrolyses sphingomyelin into ceramide. Mice deficient in either enzymes not only display perturbed hepatic levels of sphingolipids, but also an increase in hepatic triacylglycerol levels and reduced body fat compared to their wildtype counterparts ($sgpl1^{-/-}$ mice have elevated ceramide, sphingomyelin, sphingosine; $asm^{-/-}/ldlr^{-/-}$ mice have elevated ceramide, dihydroceramide, sphingomyelin; *ldlr* = low density lipoprotein receptor) [58,59]. Additionally, supplementation of liver cells with palmitate (precursor for triacylglycerol and *de novo* ceramide synthesis) stimulated triacylglycerol and sphingolipid synthesis, whereas inhibition of ASM shifted the incorporation of palmitate from triacylglycerol to ceramide [59]. Therefore, the increased level of triacylglycerol induced by ENZ-SPHK inhibition is consistent with the redirection of lipid precursors towards triacylglycerol synthesis to compensate for the accumulation of sphingosine.

Compared to SPHK1 inhibition (PF5), the effects of SPHK2 inhibition (ABC) on triacylglycerol levels were less apparent. Furthermore, sphingosine levels were not significantly increased by SPHK2 inhibition unlike SPHK1 inhibition, suggesting that phosphorylation of sphingosine into S1P is mainly catalysed by cytoplasmic SPHK1 rather than nuclear SPHK2. Thus, accumulation of cytoplasmic sphingosine by SPHK1 inhibition may be the main driver of lipogenesis-induced ER stress, resulting in a larger increase of triacylglyerols levels compared to SPHK2 inhibition.

The transcriptomic and lipidomic changes produced by ENZ-SPHK2 inhibition also differed from SPHK1 inhibition, which may be related to the different roles of S1P in the nucleus versus cytoplasm. S1P produced in the nucleus by SPHK2 can enhance histone acetylation by inhibiting the activity of histone deacetylases HDAC1 and HDAC2 [60]. Histone acetylation is typically associated with open chromatin conformation and increased gene expression, thus inhibition of SPHK2 may be disrupting the regulation of gene expression by histone deacetylases. Additionally, a different mechanism of enhanced lipogenesis under SPHK inhibition appears to be occurring for 22Rv1 which did not display SREBP1 activation, and underwent autophagy with SPHK1 inhibition. These findings demonstrate the heterogeneity of prostate cancer cells and the importance of studying different cell lines.

ABC, also known as opaganib, is the only sphingosine kinase inhibitor that has undergone clinical trials [61]. PF5 was developed by Pfizer, but never entered human trials. ABC has undergone a Phase 1 study for advanced solid tumours and was well-tolerated at 500 mg bid with the most common drug-related toxicities being nausea, vomiting and fatigue [61]. There are ongoing Phase 2 clinical trials with ABC in cancer and COVID-19.

The limitations of our study include the lack of ethnic diversity in the cohorts and the need for an independent validation cohort. More than 90% of the study cohort were Caucasians, and recruited from an Australian population, in which there is little African ancestry. The

range of life-prolonging treatment used is comparable to other developed countries in Europe and North America. However, the prognostic relationship of the circulating lipids with ARSI resistance will require validation in an independent external cohort of men of other ethnicity who may have divergent results.

In conclusion, elevated circulating ceramides were associated with ARSI resistance and confer a worse prognosis in the presence of *AR* aberrations. SPHK inhibition enhanced ENZ efficacy in PC cells. Overall, our findings indicate that ARSI resistance is mediated not only by genetic anomalies in *AR*, but also by perturbations in sphingolipid metabolism, and thus men with mCRPC might benefit from combination therapy targeting both AR signalling and sphingolipid metabolism. Further investigation with prospective clinical trials is warranted.

Contributors

H.-M.L. – conception & design, acquisition of data, analysis and interpretation of data, statistical analysis, drafting of manuscript; B.M. – analysis and interpretation of data, statistical analysis, drafting of manuscript, review & editing; N.Y. – methodology, acquisition of data, analysis and interpretation of data, review & editing; K.H., T.M., N.M. – acquisition of data, review & editing; E.M.K. – acquisition of data, analysis and interpretation of data, review & editing; H.F. – acquisition of data, analysis and interpretation of data, review & editing; B.T., I.D.D., K.L.M., A.Z., M.R.S., K.B., G.M., M.C. – acquisition of data, review & editing; P.D.S. – resources; P.D., J.Y., S.J. – acquisition of data, analysis and interpretation of data, review & editing; T.S., M.F., P.B., D.R.S. – methodology, acquisition of data, review & editing; A.M.J. – acquisition of data, review & editing; A.A.A, – administrative support, review & editing; L.M.B. – review & editing; P.J.M – acquisition of data, administrative support, review & editing; L.G.H – conception and design, acquisition of data, analysis and interpretation of data, drafting of the manuscript, review & editing, obtaining funding, administrative support, supervision.

All authors have approved the manuscript. The data in the study have been verified by H.-M.L, B.M., N.Y., K.H, T.M., N.M., E.M.K., H.F., B.T., I.D.D., K.L.M., A.Z., M.R.S., K.B., G.M., M.C., P.D., J.Y., S.J., T.S., M.F., D.R.S. A.M.J., and P.J.M.

Declaration of Competing Interest

E.M.K.: Honoraria – Janssen, Ipsen, Astellas Pharma, Research Review; Consulting or Advisory Role – Astellas Pharma, Janssen, Ipsen; Research Funding – Astellas Pharma, AstraZeneca; Travel & accommodation – Astellas Pharma, Pfizer, Ipsen, Roche.B.T.: Grants and personal fees – Amgen, AstraZeneca, Astellas, BMS, Janssen, Pfizer, MSD, Ipsen, Bayer; Personal fees – IQVIA, Sanofi, Tolmar, Novartis, Roche.A.Z.: Advisory Role – Astellas; Honoraria – Astellas; Grants and personal fees – Astra Zeneca, Pfizer; Personal fees – Merck Sharp & Dome, Bayer, Mundipharma, Janssen.I.D.D.: Institutional funding – Pfizer, ANZUP Cancer Trials Group, Bayer, Astellas, Janssen, Movember Foundation, Merck Sharp & Dome; Unremunerated chair of ANZUP Cancer Trials Group.T.S.: Travel – Astra Zeneca. D.R.S.: Grants – Regeneron, Amgen, Arrowhead, Espirion, Novartis; Personal fees – Amgen, Sanofi.A.A.: Consultant – Astellas, Janssen, Novartis; Speakers Bureau – Astellas, Janssen, Novartis, Amgen, Ipsen, Bristol Myers Squibb; Merck Serono, Bayer; Honoraria – Astellas, Novartis, Sanofi, AstraZeneca, Tolmar, Telix, Merck Serono; Janssen, Bristol Myers Squibb, Ipsen, Bayer, Pfizer, Amgen, Noxopharm, Merck Sharpe Dome; Scientific Advisory Board – Astellas, Novartis, Sanofi, AstraZeneca, Tolmar, Pfizer, Telix, Merck Serono; Janssen, Bristol Myers Squibb, Ipsen, Bayer, Merck Sharpe Dome, Amgen, Noxopharm; Travel & accommodation – Astellas, Merck Serono, Amgen, Novartis, Janssen, Tolmar, Pfizer; Investigator research funding – Astellas, Merck Serono, Astra Zeneca; Institutional research funding – Bristol Myers Squibb, Astra Zeneca, Aptevo Therapeutics, Glaxo Smith Kline, Pfizer, MedImmune, Astellas, SYNthorx, Bionomics, Sanofi Aventis, Novartis, Ipsen.A.M.J.: Insitutional funding – Pfizer, Astellas.L.G.H.: Research funding – Astellas; Travel sponsorship – Janssen, Pfizer; Honoraria – Imagion Biosystems.

All other authors have declared no conflicts of interest.

Acknowledgments

We gratefully acknowledge Lisa Graham (Chris O'Brien Lifehouse), Anne-Maree Hayes (Garvan Institute of Medical Research), Daniela Barreto (Garvan Institute of Medical Research) and research nurses for collection of blood/tissue specimens and clinical data; Gillian Lehrbach for assistance with tissue culture; Anaiis Zaratzian and Garvan Histopathology staff for assistance with immunostaining of tissue; and Tony Maxwell as our consumer representative.

We also thank our funders: National Health and Medical Research Council of Australia (GNT0614296 & APP1196225 to L.G.H, GNT1098647 to A.A.A); Cancer Institute New South Wales (10/TPG/1-04 & 2018/TPG001 to L.G.H); Australian Prostate Cancer Research Centre-New South Wales; Australian Department of Health and Aging; the Movember Foundation and the Prostate Cancer Foundation of Australia (Revolutionary Team Award MRTA3 to L.M.B and L.G.H); Cancer Council New South Wales (PG 10-01 to L.G.H); Cancer Council South Australia (Beat Cancer Project Principal Cancer Research Fellowship, PRF1117 to L.M.B); The Victorian Government's Operational Infrastructure Support Program; NHMRC Postgraduate Scholarship (E.M.K), Monash University Postgraduate Publications Award (E.M.K & H.F); Cancer Council Victoria Postdoctoral Fellowship (E.M.K); Australian Government Research Training Program Scholarship (H.F); Victorian Cancer Agency Clinical Research Fellowship (CRF14009 to A.A.A); Astellas Investigator-Initiated Grant (A.A.A); Australian and New Zealand Urogenital and Prostate Cancer Trials Group's Noel Castan Fellowship (H.M.L); Twin Towns Services Community Foundation (L.G.H).

Data sharing statement

All relevant data are included in Supplementary Information. Microarray datafiles are available on Gene Omnibus Expression (GEO accession GSE173886).

Supplementary materials

Supplementary material associated with this article can be found in the online version at doi:10.1016/j.ebiom.2021.103625.

References

[1] Bray F, Ferlay J, Soerjomataram I, Siegel RL, Torre LA, Jemal A. Global cancer statistics 2018: GLOBOCAN estimates of incidence and mortality worldwide for 36 cancers in 185 countries. CA Cancer J Clin 2018;68(6):394–424.

[2] de Bono JS, Logothetis CJ, Molina A, Fizazi K, North S, Chu L, et al. Abiraterone and increased survival in metastatic prostate cancer. N Engl J Med 2011;364(21):1995–2005.

[3] Scher HI, Fizazi K, Saad F, Taplin ME, Sternberg CN, Miller K, et al. Increased survival with enzalutamide in prostate cancer after chemotherapy. N Engl J Med 2012;367(13):1187–97.

[4] Beer TM, Armstrong AJ, Rathkopf DE, Loriot Y, Sternberg CN, Higano CS, et al. Enzalutamide in metastatic prostate cancer before chemotherapy. N Engl J Med 2014;371(5):424–33.

[5] Ryan CJ, Smith MR, Fizazi K, Saad F, Mulders PF, Sternberg CN, et al. Abiraterone acetate plus prednisone versus placebo plus prednisone in chemotherapy-naive men with metastatic castration-resistant prostate cancer (COU-AA-302): final overall survival analysis of a randomised, double-blind, placebo-controlled phase 3 study. Lancet Oncol 2015;16(2):152–60.

[6] Buttigliero C, Tucci M, Bertaglia V, Vignani F, Bironzo P, Di Maio M, et al. Understanding and overcoming the mechanisms of primary and acquired resistance to abiraterone and enzalutamide in castration resistant prostate cancer. Cancer Treat Rev 2015;41(10):884–92.

[7] Watson PA, Arora VK, Sawyers CL. Emerging mechanisms of resistance to androgen receptor inhibitors in prostate cancer. Nat Rev Cancer 2015;15(12):701–11.
[8] Azad AA, Volik SV, Wyatt AW, Haegert A, Le Bihan S, Bell RH, et al. Androgen receptor gene aberrations in circulating cell-free DNA: biomarkers of therapeutic resistance in castration-resistant prostate cancer. Clin Cancer Res 2015;21(10):2315–24.
[9] Formaggio N, Rubin MA, Theurillat JP. Loss and revival of androgen receptor signaling in advanced prostate cancer. Oncogene 2021;40(7):1205–16.
[10] Ogretmen B. Sphingolipid metabolism in cancer signalling and therapy. Nat Rev Cancer 2018;18(1):33–50.
[11] Pyne NJ, Pyne S. Sphingosine 1-phosphate and cancer. Nat Rev Cancer 2010;10(7):489–503.
[12] Spiegel S, Milstien S. The outs and the ins of sphingosine-1-phosphate in immunity. Nat Rev Immunol 2011;11(6):403–15.
[13] Raval AD, Thakker D, Negi H, Vyas A, Salkini MW. Association between statins and clinical outcomes among men with prostate cancer: a systematic review and meta-analysis. Prostate Cancer Prostatic Dis 2016;19(2):151–62.
[14] Van Rompay MI, Solomon KR, Nickel JC, Ranganathan G, Kantoff PW, McKinlay JB. Prostate cancer incidence and mortality among men using statins and non-statin lipid-lowering medications. Eur J Cancer 2019;112:118–26.
[15] Carretero-González A, Lora D, Manneh R, Lorente D, Castellano D, de Velasco G. Combination of statin/vitamin D and metastatic castration-resistant prostate cancer (CRPC): a post hoc analysis of two randomized clinical trials. Clin Transl Oncol 2020;22(11):2126–9.
[16] Di Lorenzo G, Sonpavde G, Pond G, Lucarelli G, Rossetti S, Facchini G, et al. Statin use and survival in patients with metastatic castration-resistant prostate cancer treated with abiraterone acetate. Eur Urol Focus 2018;4(6):874–9.
[17] Wu SY, Fang SC, Shih HJ, Wen YC, Shao YHJ. Mortality associated with statins in men with advanced prostate cancer treated with androgen deprivation therapy. Eur J Cancer 2019;112:109–17.
[18] Arthur R, Møller H, Garmo H, Häggström C, Holmberg L, Stattin P, et al. Serum glucose, triglycerides, and cholesterol in relation to prostate cancer death in the Swedish AMORIS study. Cancer Causes Control 2019;30(2):195–206.
[19] Allott EH, Howard LE, Cooperberg MR, Kane CJ, Aronson WJ, Terris MK, et al. Serum lipid profile and risk of prostate cancer recurrence: results from the SEARCH database. Cancer Epidemiol Biomark Prev 2014;23(11):2349–56.
[20] Cheng S, Zheng Q, Ding G, Li G. Influence of serum total cholesterol, LDL, HDL, and triglyceride on prostate cancer recurrence after radical prostatectomy. Cancer Manag Res 2019;11:6651–61.
[21] Meikle PJ, Wong G, Tan R, Giral P, Robillard P, Orsoni A, et al. Statin action favors normalization of the plasma lipidome in the atherogenic mixed dyslipidemia of MetS: potential relevance to statin-associated dysglycemia. J Lipid Res 2015;56(12):2381–92.
[22] Ng TW, Ooi EM, Watts GF, Chan DC, Weir JM, Meikle PJ, et al. Dose-dependent effects of rosuvastatin on the plasma sphingolipidome and phospholipidome in the metabolic syndrome. J Clin Endocrinol Metab 2014;99(11):E2335–40.
[23] Tarasov K, Ekroos K, Suoniemi M, Kauhanen D, Sylvanne T, Hurme R, et al. Molecular lipids identify cardiovascular risk and are efficiently lowered by simvastatin and PCSK9 deficiency. J Clin Endocrinol Metab 2014;99(1):E45–52.
[24] Lin HM, Mahon KL, Weir JM, Mundra PA, Spielman C, Briscoe K, et al. A distinct plasma lipid signature associated with poor prognosis in castration-resistant prostate cancer. Int J Cancer 2017;141(10):2112–20.
[25] Lin HM, Huynh K, Kohli M, Tan W, Azad AA, Yeung N, et al. Aberrations in circulating ceramide levels are associated with poor clinical outcomes across localised and metastatic prostate cancer. Prostate Cancer Prostatic Dis 2021;24(3):860–70.
[26] Lucki NC, Sewer MB. The interplay between bioactive sphingolipids and steroid hormones. Steroids 2010;75(6):390–9.
[27] Kwun C, Patel A, Pletcher S, Lyons B, Abdelrahim M, Nicholson D, et al. Ceramide increases steroid hormone production in MA-10 Leydig cells. Steroids 1999;64(8):499–509.
[28] Ozbay T, Rowan A, Leon A, Patel P, Sewer MB. Cyclic adenosine 5′-monophosphate-dependent sphingosine-1-phosphate biosynthesis induces human CYP17 gene transcription by activating cleavage of sterol regulatory element binding protein 1. Endocrinology 2006;147(3):1427–37.
[29] Urs AN, Dammer E, Sewer MB. Sphingosine regulates the transcription of CYP17 by binding to steroidogenic factor-1. Endocrinology 2006;147(11):5249–58.
[30] Lightle S, Tosheva R, Lee A, Queen-Baker J, Boyanovsky B, Shedlofsky S, et al. Elevation of ceramide in serum lipoproteins during acute phase response in humans and mice: role of serine-palmitoyl transferase. Arch Biochem Biophys 2003;419(2):120–8.
[31] Santos WL, Lynch KR. Drugging sphingosine kinases. ACS Chem Biol 2015;10(1):225–33.
[32] Spiegel S, Milstien S. Functions of the multifaceted family of sphingosine kinases and some close relatives. J Biol Chem 2007;282(4):2125–9.
[33] Malavaud B, Pchejetski D, Mazerolles C, de Paiva GR, Calvet C, Doumerc N, et al. Sphingosine kinase-1 activity and expression in human prostate cancer resection specimens. Eur J Cancer 2010;46(18):3417–24.
[34] Zhang Y, Wang Y, Wan Z, Liu S, Cao Y, Zeng Z. Sphingosine kinase 1 and cancer: a systematic review and meta-analysis. PLoS One 2014;9(2):e90362.
[35] Pchejetski D, Bohler T, Stebbing J, Waxman J. Therapeutic potential of targeting sphingosine kinase 1 in prostate cancer. Nat Rev Urol 2011;8(10):569–678.
[36] Schrecengost RS, Keller SN, Schiewer MJ, Knudsen KE, Smith CD. Downregulation of critical oncogenes by the selective SK2 inhibitor ABC294640 hinders prostate cancer progression. Mol Cancer Res 2015;13(12):1591–601.
[37] Pchejetski D, Doumerc N, Golzio M, Naymark M, Teissie J, Kohama T, et al. Chemosensitizing effects of sphingosine kinase-1 inhibition in prostate cancer cell and animal models. Mol Cancer Ther 2008;7(7):1836–45.
[38] Dayon A, Brizuela L, Martin C, Mazerolles C, Pirot N, Doumerc N, et al. Sphingosine kinase-1 is central to androgen-regulated prostate cancer growth and survival. PLoS One 2009;4(11):e8048.
[39] Scher HI, Halabi S, Tannock I, Morris M, Sternberg CN, Carducci MA, et al. Design and end points of clinical trials for patients with progressive prostate cancer and castrate levels of testosterone: recommendations of the prostate cancer clinical trials working group. J Clin Oncol 2008;26(7):1148–59.
[40] Huynh K, Barlow CK, Jayawardana KS, Weir JM, Mellett NA, Cinel M, et al. High-throughput plasma lipidomics: detailed mapping of the associations with cardiometabolic risk factors. Cell Chem Biol 2019;26(1):71–84 e4.
[41] Fettke H, Kwan EM, Docanto MM, Bukczynska P, Ng N, Graham LK, et al. Combined cell-free DNA and RNA profiling of the androgen receptor: clinical utility of a novel multianalyte liquid biopsy assay for metastatic prostate cancer. Eur Urol 2020;78(2):173–80.
[42] Centenera MM, Gillis JL, Hanson AR, Jindal S, Taylor RA, Risbridger GP, et al. Evidence for efficacy of new Hsp90 inhibitors revealed by *ex vivo* culture of human prostate tumors. Clin Cancer Res 2012;18(13):3562–70.
[43] Weir JM, Wong G, Barlow CK, Greeve MA, Kowalczyk A, Almasy L, et al. Plasma lipid profiling in a large population-based cohort. J Lipid Res 2013;54(10):2898–908.
[44] Abida W, Cyrta J, Heller G, Prandi D, Armenia J, Coleman I, et al. Genomic correlates of clinical outcome in advanced prostate cancer. Proc Natl Acad Sci U S A 2019;116(23):11428–36.
[45] Ritchie ME, Phipson B, Wu D, Hu Y, Law CW, Shi W, et al. limma powers differential expression analyses for RNA-sequencing and microarray studies. Nucleic Acids Res. 2015;43(7):e47. e.
[46] Liberzon A, Subramanian A, Pinchback R, Thorvaldsdóttir H, Tamayo P, Mesirov JP. Molecular signatures database (MSigDB) 3.0. Bioinformatics 2011;27(12):1739–40.
[47] Subramanian A, Tamayo P, Mootha VK, Mukherjee S, Ebert BL, Gillette MA, et al. Gene set enrichment analysis: a knowledge-based approach for interpreting genome-wide expression profiles. Proc Natl Acad Sci U S A 2005;102(43):15545–50.
[48] Książek M, Chacińska M, Chabowski A, Baranowski M. Sources, metabolism, and regulation of circulating sphingosine-1-phosphate. J Lipid Res 2015;56(7):1271–81.
[49] Shimano H, Sato R. SREBP-regulated lipid metabolism: convergent physiology — divergent pathophysiology. Nat Rev Endocrinol 2017;13(12):710–30.
[50] French KJ, Zhuang Y, Maines LW, Gao P, Wang W, Beljanski V, et al. Pharmacology and antitumor activity of ABC294640, a selective inhibitor of sphingosine kinase-2. J Pharmacol Exp Ther 2010;333(1):129–39.
[51] Nagahashi M, Yamada A, Katsuta E, Aoyagi T, Huang WC, Terracina KP, et al. Targeting the SphK1/S1P/S1PR1 axis that links obesity, chronic inflammation, and breast cancer metastasis. Cancer Res 2018;78(7):1713–25.
[52] Cuvillier O, Edsall L, Spiegel S. Involvement of sphingosine in mitochondria-dependent Fas-induced apoptosis of type II Jurkat T cells. J Biol Chem 2000;275(21):15691–700.
[53] Lurlaro R, Muñoz-Pinedo C. Cell death induced by endoplasmic reticulum stress. Febs J 2016;283(14):2640–52.
[54] Sheng X, Nenseth HZ, Qu S, Kuzu OF, Frahnow T, Simon L, et al. IRE1α-XBP1s pathway promotes prostate cancer by activating c-MYC signaling. Nat Commun 2019;10(1):323.
[55] Lima S, Milstien S, Spiegel S. Sphingosine and sphingosine kinase 1 involvement in endocytic membrane trafficking. J Biol Chem 2017;292(8):3074–88.
[56] Han J, Kaufman RJ. The role of ER stress in lipid metabolism and lipotoxicity. J Lipid Res 2016;57(8):1329–38.
[57] Kim JY, Garcia-Carbonell R, Yamachika S, Zhao P, Dhar D, Loomba R, et al. ER stress drives lipogenesis and steatohepatitis via caspase-2 activation of S1P. Cell 2018;175(1):133–45 e15.
[58] Bektas M, Allende ML, Lee BG, Chen W, Amar MJ, Remaley AT, et al. Sphingosine 1-phosphate lyase deficiency disrupts lipid homeostasis in liver. J Biol Chem 2010;285(14):10880–9.
[59] Deevska GM, Rozenova KA, Giltiay NV, Chambers MA, White J, Boyanovsky BB, et al. Acid sphingomyelinase deficiency prevents diet-induced hepatic triacylglycerol accumulation and hyperglycemia in mice. J Biol Chem 2009;284(13):8359–68.
[60] Hait NC, Allegood J, Maceyka M, Strub GM, Harikumar KB, Singh SK, et al. Regulation of histone acetylation in the nucleus by sphingosine-1-phosphate. Science 2009;325(5945):1254–7.
[61] Britten CD, Garrett-Mayer E, Chin SH, Shirai K, Ogretmen B, Bentz TA, et al. A phase I study of ABC294640, a first-in-class sphingosine kinase-2 inhibitor, in patients with advanced solid tumors. Clin Cancer Res 2017;23(16):4642–50.